2 mif

eirs

ENGINEERING & INDUSTRIAL RESEARCH STATION

MECHANICAL ENGINEERING / MISSISSIPPI STATE UNIVERSITY

(NASA-CR-138307) STIFFNESS AND DAMPING OF AN INHERENTLY COMPENSATED GAS LUBRICATED BEARING OF SQUARE GEOMETRY Annual Report, Jan. - Dec. 1973 (Mississippi State Univ.) 6564 p CSCL 13I G3/15

N74-29927

Unclas 45717

STIFFNESS AND DAMPING OF AN INHERENTLY COMPENSATED GAS LUBRICATED BEARING OF SQUARE GEOMETRY

NATIONAL AERONAUTICS AND SPACE ADMINISTRATION

GRANT NGR 25-001-050, SUPPLEMENT NO.1

BY

A. KENT STIFFLER

DAVID M. SMITH

EIRS-ME-75-1

COLLEGE OF ENGINEERING ADMINISTRATION

HARRY C. SIMRALL, M.S.
DEAN, COLLEGE OF ENGINEERING

WILLIE L. MCDANIEL, JR., PH.D.
ASSOCIATE DEAN

WALTER R. CARNES, PH.D.
ASSOCIATE DEAN

LAWRENCE J. HILL, M.S.
DIRECTOR, ENGINEERING EXTENSION

CHARLES B. CLIETT, M.S.
AEROPHYSICS & AEROSPACE ENGINEERING

WILLIAM R. FOX, PH.D.
AGRICULTURAL & BIOLOGICAL ENGINEERING

JOHN L. WEEKS, JR., PH.D.
CHEMICAL ENGINEERING

ROBERT M. SCHOLTES, PH.D.
CIVIL ENGINEERING

B. J. BALL, PH.D.
ELECTRICAL ENGINEERING

W. H. EUBANKS, M.ED.
ENGINEERING GRAPHICS

J. E. THOMAS, M.S.
INSTITUTE OF ENGINEERING TECHNOLOGY

FRANK E. COTTON, JR., PH.D.
INDUSTRIAL ENGINEERING

C. T. CARLEY, PH.D.
MECHANICAL ENGINEERING

JOHN I. PAULK, PH.D.
NUCLEAR ENGINEERING

WILLIAM D. MCCAIN, JR., PH.D.
PETROLEUM ENGINEERING

For additional copies or information
address correspondence to:

ENGINEERING AND INDUSTRIAL RESEARCH STATION
DRAWER DE
MISSISSIPPI STATE UNIVERSITY
MISSISSIPPI STATE, MISSISSIPPI 39762

TELEPHONE (601) 325-2266

Stiffness and Damping of an Inherently Compensated
Gas Lubricated Bearing of Square Geometry

by

A. Kent Stiffler, Principal Investigator
David M. Smith

Department of Mechanical Engineering

Supported by National Aeronautics and Space Administration

Grant NGR 25-001-050, Supplement No. 1

Mississippi State University

Engineering and Industrial Research Station

Mississippi State, Mississippi 39762

Annual Report

January 1973 to December 1973

ii

ABSTRACT

The load, mass flow, stiffness, and damping for an inherently compensated, multiple-inlet, externally pressurized square thrust bearing are analyzed. Small perturbation methods are used to linearize Reynolds' equation, and numberical methods are employed to find the solution to the resulting equations. Design curves are presented in terms of restrictor coefficient, supply pressure, and location of the inlets for low squeeze numbers.

Optimum bearing stiffness occurs at a restrictor coefficient between one and two. At this value the damping is a minimum and negative damping (instability) can be present at supply pressures exceeding four atmospheres. Stiffness increases with supply pressure. Optimum damping occurs at a restrictor coefficient equal to five. Stiffness is considerably reduced but can be improved by operating at high supply pressures.

PRECEDING PAGE BLANK NOT FILMED

TABLE OF CONTENTS

LIST OF FIGURES

NOMENCLATURE

SYMBOL	DESCRIPTION
*	Denotes real variable
α	Iteration count
β	Increment ratio (Length/Width -- $\Delta x/\Delta z$)
ε	Perturbation parameter
γ	Normalized span across outer sill
λ	Dimensionless width (Bearing width/Bearing length)
Λ	Restrictor Coefficient
μ	Fluid viscosity
ω^*	Excitation frequency
ρ^*	Density of film
σ	Squeeze number $\left(\frac{12\mu\omega^* L^{*2}}{h_o^{*2}\ P_a^*} \right)$
a	Maximum value of x on the boundary $\left(\frac{1-2\gamma}{2}\right)$
b	Maximum value of z on the boundary $\left(\frac{\lambda-2\gamma}{2}\right)$
C_D	Orifice discharge coefficient
d_o^*	Orifice diameter
D^*	Damping
D	Dimensionless damping $[D^*/(\lambda L^*\mu (L^*/h_o^*)^3)]$
F	$\int_o^a \left(\frac{\partial \overline{P}_1}{\partial z}\right)^2_{z=b+} dx + \int_o^b \left(\frac{\partial \overline{P}_1}{\partial x}\right)^2_{x=a+} dz$
g	$[P_1(x,z)P_2(x,z,t)]$
g_o	Acceleration of gravity
h^*	Film thickness
h_o^*	Mean film thickness
h	Dimensionless film thickness

NOMENCLATURE (continued)

SYMBOL	DESCRIPTION
i	Row number in numerical field
j	Column number in numerical field
k	Ratio of specific heats ($\frac{c_p}{c_v}$)
K^*	Stiffness
K_S	Dimensionless stiffness [$K^* h_o^*/(\lambda P^*_a L^{*2}(P_s-1))$]
L^*	Bearing length
m_o^*	Mean mass flow
m_1^*	Dynamic mass flow through orifice
m_2^*	Dynamic mass flow through outer sill
m_3^*	Dynamic mass flow from central region
M_1^*	Mass flow through orifice
M_2^*	Mass flow through outer sill
M_3^*	Mass flow from central region
N_a	Maximum column number at inlet boundary
N_b	Maximum row number at inlet boundary
N_1	Number of inlets
P^*	Pressure
P	Dimensionless pressure (P^*/P^*_a)
P^*_a	Ambient pressure
P_1	Dimensionless static pressure
P_2	Dimensionless dynamic pressure
P_i	Dimensionless dynamic pressure downstream of inlet
P_o	Dimensionless static pressure downstream of inlet
P_s	Dimensionless supply pressure
r	Inlet span to total bearing span ratio

NOMENCLATURE (continued)

SYMBOL	DESCRIPTION
R	Gas constant
t^*	Time
t	Dimensionless time $(t^*\omega^*)$
T	Temperature
W^*	Bearing load
W	Dimensionless bearing load $(W^*/\lambda P^*_a L^{*2})$
W_1^*	Static load
W_1	Dimensionless static load
W_2^*	Dynamic load
W_2	Dimensionless dynamic load
x^*	Variable length
x	Dimensionless variable length (x^*/L^*)
z^*	Variable width
z	Dimensionless variable width (z^*/L^*)

CHAPTER I

INTRODUCTION

Energy loss and the wear of machine parts due to friction are two of the problems which are faced in industry every day. Fluid film bearings are used at critical areas to reduce this friction. The fluids used in these bearings are usually a gas or oil. With the reduction of friction, the lives of the machines are lengthened which saves the industries large amounts of money both in labor and shut-down time.

The two basic types of bearings used in industry are the thrust bearing and the journal bearing. The journal bearing supports radial loads; whereas, the thrust bearing supports an axial load. In some cases, thrust bearings have been used in conjunction with journal bearings to provide damping for radial loads.

A bearing load can be supported hydrodynamically or hydrostatically. In hydrodynamic lubrication, Figure 1(a), high pressure is developed when the fluid film is "dragged" along as a wedge. The fluid film in a hydrostatic bearing must be externally pressurized to support a load. The externally pressurized bearing may be either orifice compensated, Figure 1(b), or inherently compensated, Figure 1(c). Each of these geometries has a flow inlet restriction area which controls the flow through the bearing. The "restrictor" is dependent upon the orifice area in the orifice compensated case and is dependent upon the hole diameter and film thickness in the inherently compensated case.

In recent years, there has been a rapid growth in the development of gas bearing supported systems. The reason for this growth is that industry is beginning to recognize the many advantages of gas

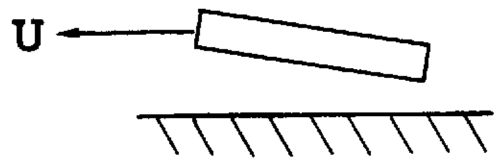

(a) Hydrodynamic Lubrication

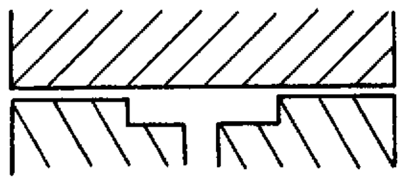

(b) Hydrostatic Lubrication-Orifice Compensated

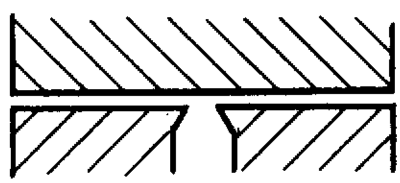

(c) Hydrostatic Lubrication-Inherent Compensation

Figure 1. Examples of Gas Lubrication.

lubrication. One of the most appealing advantages is the use of a process fluid as the lubricant. This eliminates the need for an external lubrication system. Some of the other advantages of gas lubrication are: lower friction, no contamination, low-to-high temperature capability, high speed capability, and high reliability and long life.

The response of gas bearings to small periodic load changes is greatly influenced by the dynamic characteristics of the gas film. Stiffness and damping are important parameters which affect this dynamic behavior of the system. Stability problems arise when there is negative damping present. Although inherently compensated bearings have less stiffness than pocket-type bearings, they do exhibit improved stability over the pocket-type bearings which are prone to pneumatic hammer [1]*.

Richardson [1] was one of the first to carry out a theoretical analysis of the dynamic characteristics of an orifice compensated gas bearing. Using lumped parameter methods, he developed relationships which could be used to obtain quantitative design information for compensated gas bearings. Licht and Elrod [2] analyzed the stability of an orifice compensated bearing similar to the one studied by Richardson using distributed parameter methods. There was a marked divergence from the results obtained by lumped parameter methods in the case of the limiting values which influence the stability of the bearing. Stiffler [3] has presented an analysis of an inherently compensated, multiple-inlet, circular thrust bearing based on distributed parameter methods. In his solutions, the stiffness and damping as

*Numbers in brackets refer to references functions of supply pressure, inlet location, restrictor coefficient, and excitation frequency are described by perturbation models.

Mullan and Richardson [4] used lumped and distributed parameter analyses to develop solutions for the inherently compensated gas journal bearing with small eccentricity ratios. After linearizing Reynolds' equation using small perturbation methods, the computer was used to obtain results which were presented in graphical form with stiffness and damping as functions of supply pressure and flow. Lund [5] presented a theoretical analysis for the threshold of instability of a rigid rotor supported in hydrostatic gas journal bearings. Perturbation techniques were used, and numerical results were given for the threshold of instability as a function of supply pressure ratio, restrictor coefficient and eccentricity ratio.

This thesis deals with an externally pressurized, inherently compensated, multiple-inlet, square thrust bearing. A mathematical model is formulated for the general rectangular case, as shown in Figure 2, with the bearing dimensions normalized by the bearing length. Thus, the bearing is of unit length and has a width, λ, where λ is the actual bearing width divided by the length. The nonlinear Reynolds' equation is solved using small perturbation techniques. Design curves for the stiffness, damping, load, and mass flow are presented as functions of inlet location, restrictor coefficient, and supply pressure for small squeeze numbers. A theoretical analysis of these bearing characteristics is developed in the following section.

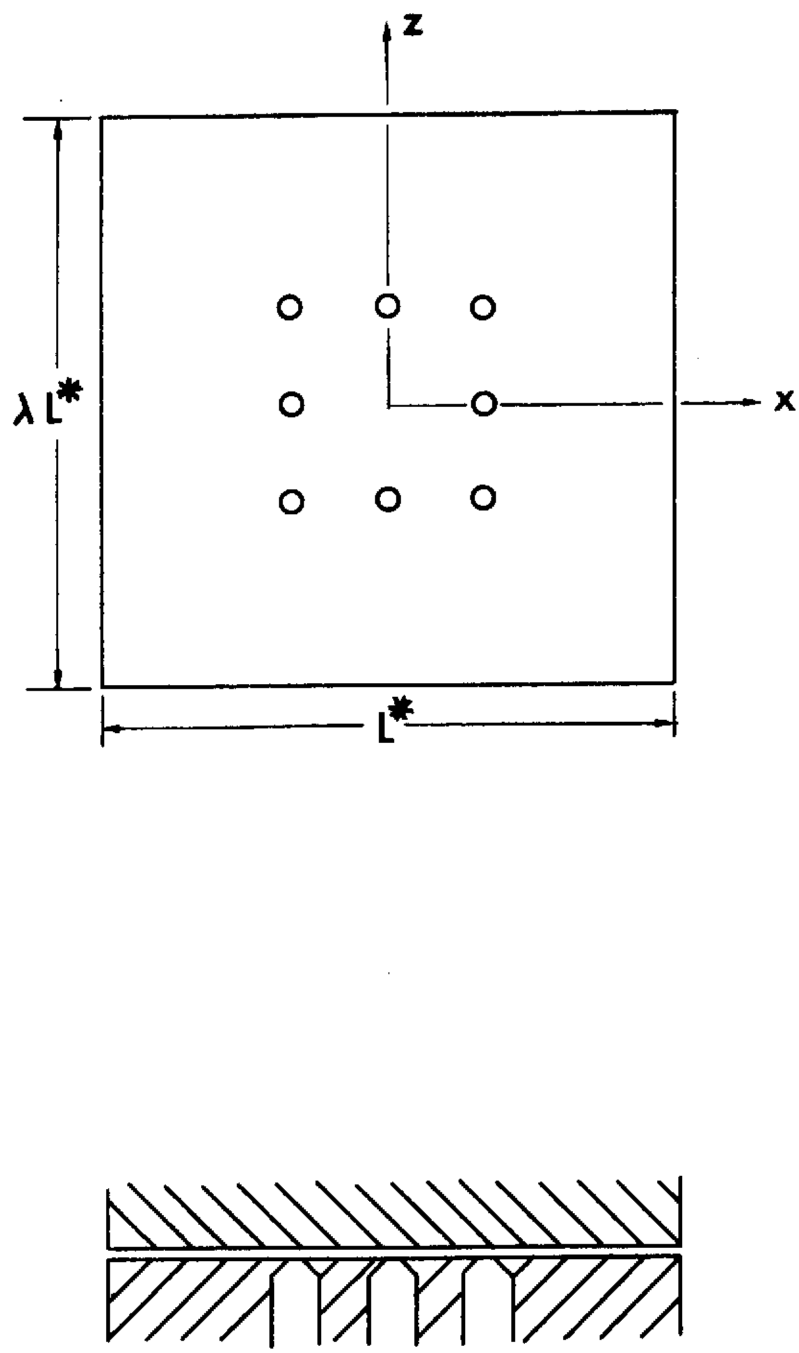

Figure 2. Inherently Compensated, Multiple-Inlet, Rectangular Thrust Bearing.

CHAPTER II

FORMULATION OF THE MATHEMATICAL MODEL

For the development of the theoretical model, the bearing is divided into three distinct regions--the inlet region, the central region, and the sill region. The gas lubricant flows through the sill and attains an ambient state at the outer edges of the sill. It is assumed that there are enough inlets so that they may be considered as an equivalent line source. Furthermore, only one quadrant is considered since the bearing is symmetric.

2.1 Reynolds' Equation Applied to the Bearing

In order to solve for the mass flow, load, stiffness, and damping, the pressure distribution throughout the bearing must be determined. The pressure distribution is described by Reynolds' equation

$$\frac{\partial}{\partial x^*}\left(h^{*3}\rho^*\frac{\partial P^*}{\partial x^*}\right)+\frac{\partial}{\partial z^*}\left(h^{*3}\rho^*\frac{\partial P^*}{\partial z^*}\right)=12\mu\frac{\partial}{\partial t^*}(\rho^* h^*) \tag{2-1}$$

The film thickness, h^*, is uniform throughout the flow region, since it is bounded by two parallel rigid surfaces. The separation of the surfaces depends only upon the load disturbance.

It is assumed in the analysis that the film behaves as an ideal gas with constant specific heats and that the flow is isothermal [6] with P^*/ρ^* = constant. The following dimensionless variables,

$$P = P^*/P_a^*$$

$$x = x^*/L^*$$

$$z = z^*/L^*$$

$$t = t^*\omega^*$$

$$h = h^*/h_o^*$$

are introduced into Reynolds' equation to obtain

$$\frac{\partial^2}{\partial x^2}(P^2) + \frac{\partial^2}{\partial z^2}(P^2) = \frac{2\sigma}{h^3}\frac{\partial}{\partial t}(Ph) \tag{2-2}$$

where the squeeze number, σ, is given by

$$\sigma = \frac{12\mu\omega^* L^{*2}}{h_o^{*2}\ P_a{}^*} \tag{2-3}$$

In terms of a perturbation parameter, ε, the film height and pressure distribution can be approximated as

$$h(t) = 1 + \varepsilon \sin(t) \tag{2-4}$$

$$P(x,z,t) = P_1(x,z) + \varepsilon P_2(x,z,t) \tag{2-5}$$

where $P_1(x,z)$ is the dimensionless static pressure distribution and $P_2(x,z,t)$ is the first order dimensionless dynamic pressure distribution.

When Equations (2-4) and (2-5) are substituted into Equation (2-2), two equations are obtained from terms of order $O(1)$ and $O(\varepsilon)$, respectively.

$$O(1):\quad \frac{\partial^2 P_1{}^2}{\partial x^2} + \frac{\partial^2 P_1^2}{\partial z^2} = 0 \tag{2-6}$$

$$O(\varepsilon):\quad \frac{\partial^2(P_1P_2)}{\partial x^2} + \frac{\partial^2(P_1P_2)}{\partial z^2} = \sigma(P_1\cos(t) + \frac{\partial P_2}{\partial t}) \tag{2-7}$$

Or, in a more convenient form, Equation (2-7) is written as

$$\frac{\partial^2 g}{\partial x^2} + \frac{\partial^2 g}{\partial z^2} = \frac{\sigma}{P_1}\left[\ P_1{}^2\ \cos(t) + \frac{\partial g}{\partial t}\ \right] \tag{2-8}$$

where

$$g(x,z,t) = P_1(x,z)\ P_2(x,z,t) \tag{2-9}$$

If the pressure at the inlet boundary is defined arbitrarily as $(P_o + \epsilon P_i)$, the remaining static conditions at the inner edges of the sill are

$$P_1\ (x,b) = P_o \qquad 0 \le x \le a$$

$$P_1\ (a,z) = P_o \qquad 0 \le z \le b$$

where

$$a = \frac{1 - 2\gamma}{2} \text{ and } b = \frac{\lambda - 2\gamma}{2}$$

At the outer edges of the sill the static pressure is ambient, and

$$P_1(x,\lambda/2) = 1 \qquad 0 \le x \le 1/2$$

$$P_1(1/2,z) = 1 \qquad 0 \le z \le \lambda/2$$

The boundary conditions for Equation (2-8) are

$$g(x,\lambda/2,\ t) = 0 \qquad 0 \le x \le 1/2$$

$$g(1/2,z,t) = 0 \qquad 0 \le z \le \lambda/2$$

$$g(x,b,t) = P_oP_i \qquad 0 \le x \le a$$

$$g(a,z,t) = P_oP_i \qquad 0 \le z \le b$$

In order to normalize the boundary conditions for Equation (2-6), let

$$P_1{}^2 = 1 + (P_o{}^2 - 1)\ \overline{P}_1{}^2 \tag{2-10}$$

Then, upon substitution into Equation (2-6),

$$\frac{\partial^2 \overline{P}_1{}^2}{\partial x^2} + \frac{\partial^2 \overline{P}_1{}^2}{\partial z^2} = 0 \tag{2-11}$$

for which the boundary conditions are given by

$$\overline{P}_1^{\,2}\ (x,\ \lambda/2) = 0$$

$$\overline{P}_1^{\,2}\ (1/2,z) = 0$$

$$\overline{P}_1^{\,2}\ (x,b) = 1$$

$$\overline{P}_1^{\,2}\ (a,z) = 1$$

The load disturbance is assumed to be periodic. Thus, time may be eliminated from Equation (2-8) by assuming a periodic solution for the dynamic pressure.

Let

$$g(x,z,t) = g_1(x,z)\ \sin(t) + g_2(x,z)\ \cos(t)\ . \tag{2-12}$$

Substituting this expression into Equation (2-8), and equating coefficients of the sine and cosine terms,

$$\frac{\partial^2 g_1}{\partial x^2} + \frac{\partial^2 g_1}{\partial z^2} = -\ \frac{\sigma g_2}{P_1} \tag{2-13}$$

$$\frac{\partial^2 g_2}{\partial x^2} + \frac{\partial^2 g_2}{\partial z^2} = +\ \frac{\sigma}{P_1}\ [P_1^{\,2} + g_1] \tag{2-14}$$

For the central region, the solution to Equation (2-11) is a constant and is given by

$$\overline{P}_1^{\,2}(x,z) = 1.$$

Along the sill, numerical methods are used to solve Equation (2-11). After the static boundary pressure, P_o, is specified, the static pressure field can be found. The dynamic and static boundary pressures, P_i and P_o, must be determined from the continuity condition for the mass flow at the inlet boundary. The solutions to the coupled Equations (2-13) and (2-14) can then be found by numerical methods.

2.2 Mass Flow

From flow continuity at the boundary,

$$M_3^* + M_1^* = M_2^*$$

where

M_1^* = mass flow through the inlets = $m_o^* + \varepsilon m_1^*$

M_2^* = mass flow through the sill region = $m_o^* + \varepsilon m_2^*$

M_3^* = mass flow from the central region = εm_3^*

and m_o^* is the mean flow through the inlets (and the sill region) for the statically loaded bearing.

The mass flow through the sill region is given by Constantinescu [7] as

$$M_2^* = -\frac{1}{12}\frac{\rho^* h^{*3}}{\mu P_o^*}\left[\int_{-a}^{a}\left(\frac{\partial P^{*2}}{\partial z}\right)_{z=b^+} dx + \int_{-b}^{b}\left(\frac{\partial P^{*2}}{\partial x}\right)_{x=a^+} dz\right] . \quad (2\text{-}15)$$

When Equations (2-4), (2-10), and (2-5) are substituted into Equation (2-15) the linearized mass flow through the sill region is

$$M_2^* = m_o^* + 3m_o^*\,\varepsilon\sin(t) + \frac{P_a^{*2} h_o^{*3}}{12\mu RT}(2\varepsilon)\left[\int_{-a}^{a}\left(\frac{\partial g}{\partial z}\right)_{z=b^+} dx + \int_{-b}^{b}\left(\frac{\partial g}{\partial x}\right)_{x=a^+} dz\right] \quad (2\text{-}16)$$

where

$$m_o^* = -\frac{P_a^{*2} h_o^{*3}}{6\mu RT}\,(P_o^{\,2} - 1)\,F \quad (2\text{-}17)$$

and

$$F = \int_{o}^{a}\left(\frac{\partial \overline{P}_1^{\,2}}{\partial z}\right)_{z=b^+} dx + \int_{o}^{b}\left(\frac{\partial \overline{P}_1^{\,2}}{\partial x}\right)_{x=a^+} dz \quad . \quad (2\text{-}18)$$

The mass flow, M_3^*, from the central region is given by the same general expression as Equation (2-15) except that the derivatives are evaluated at the inside of the inlet boundary. Thus,

$$M_3^* = - \frac{P_a^{*2} h_o^{*3}}{12\mu RT}(2\varepsilon) \left[\int_{-a}^{a} \left(\frac{\partial g}{\partial z}\right)_{z=b^-} dx + \int_{-b}^{b} \left(\frac{\partial g}{\partial x}\right)_{x=a^-} dz \right] \tag{2-19}$$

where the mean flow is zero.

The flow through the inlets [8] is described by

$$M_1^* = \frac{C_D N_1 \pi d_o^* h_o^* h P_s P_a^*}{\sqrt{RT}} \left[\frac{2g_o k}{k - 1} \right]^{1/2} \left(\frac{P}{P_s} \right)^{1/k} \left[1 - \left(\frac{P}{P_s}\right)^{\frac{k-1}{k}} \right]^{1/2},$$

$$\frac{P_o}{P_s} > \left(\frac{2}{k+1}\right)^{\frac{k}{k-1}} \tag{2-20}$$

or

$$M_1^* = \frac{C_D N_1 \pi d_o^* h_o^* h P_s P_a^*}{\sqrt{RT}} \left(\frac{2g_o k}{k+1} \right)^{1/2} \left(\frac{2}{k + 1} \right)^{\frac{1}{k-1}},$$

$$\frac{P_o}{P_s} \leq \left(\frac{2}{k+1}\right)^{\frac{k}{k-1}} \tag{2-21}$$

Equations (2-4) and (2-5) can be substituted into Equations (2-20) and (2-21), and, when terms of order O(1) and O(ε) are retained,

$$M_1^* = m_o^* \left\{ 1 + \left[\sin(t) + \left(\frac{P_1}{P_s}\right) \alpha_2 \right] \varepsilon \right\}, \frac{P_o}{P_s} > \left(\frac{2}{k+1}\right)^{\frac{k}{k-1}} \tag{2-22}$$

or

$$M_1^* = m_o^* + m_o^* \varepsilon\sin(t) \quad , \quad \frac{P_o}{P_s} \leq \left(\frac{2}{k+1}\right)^{\frac{k}{k-1}} \tag{2-23}$$

where

$$\alpha_2 = \frac{1}{k}\left(\frac{P_s}{P_o}\right) - \frac{k-1}{2k}\left[\frac{(P_o/P_s)^{-\frac{1}{k}}}{1-(P_o/P_s)^{\frac{k-1}{k}}}\right] \tag{2-24}$$

and

$$m_o^* = \frac{C_D N_1 \pi d_o{}^* h_o{}^* P_s P_a{}^*}{\sqrt{RT}}\left(\frac{2g_o k}{k-1}\right)^{1/2}\left(\frac{P_o}{P_s}\right)^{1/k}\left[1-\left(\frac{P_o}{P_s}\right)^{\frac{k-1}{k}}\right]^{1/2} ,$$

$$\frac{P_o}{P_s} > \left(\frac{2}{k+1}\right)^{\frac{k}{k-1}} \tag{2-25}$$

or

$$m_o{}^* = \frac{C_D N_1 \pi d_o{}^* h_o{}^* P_s P_a{}^*}{\sqrt{RT}}\left(\frac{2g_o k}{k+1}\right)^{1/2}\left(\frac{2}{k+1}\right)^{\frac{1}{k-1}} ,$$

$$\frac{P_o}{P_s} \leq \left(\frac{2}{k+1}\right)^{\frac{k}{k-1}} \tag{2-26}$$

From the continuity requirement for the mean mass flow through the bearing, and for adiabatic flow through the orifice, P_o is given by

$$1 = \frac{\Lambda}{P_o^2-1}\left(\frac{P_o}{P_s}\right)^{1/k} P_s{}^2\left[1-\left(\frac{P_o}{P_s}\right)^{\frac{k-1}{k}}\right]^{1/2} , \frac{P_o}{P_s} > \left(\frac{2}{k+1}\right)^{\frac{k}{k-1}} \tag{2-27}$$

and

$$P_o{}^2 = 1 + \Lambda P_s{}^2\left(\frac{k-1}{k+1}\right)^{1/2}\left(\frac{2}{k+1}\right)^{\frac{1}{k-1}} , \frac{P_o}{P_s} \leq \left(\frac{2}{k+1}\right)^{\frac{k}{k-1}} \tag{2-28}$$

where the restrictor coefficient, Λ, is

$$\Lambda = - \frac{6\ C_D N_1 \pi d_o^{*} \mu}{P_s P_a^{*} h_o^{*2} F} \left[\frac{2 g_o k R T}{(k-1)}\right]^{1/2}$$

and F is given by Equation (2-18). The restrictor coefficient, Λ, is a dimensionless parameter which gives an indication of the resistance to the mass flow through the orifice and the sill. As the restrictor coefficient increases, the resistance to mass flow increases.

The pressure downstream of the orifice, P_o, is directly affected by the restrictor coefficient. An increase in the restrictor coefficient results in an increase in the pressure downstream of the orifice. If the flow is not critical, a Newton-Raphson method is used to solve Equation (2-27) for P_o, or if the flow is critical, P_o is obtained directly from Equation (2-28). Once P_o is found, the static pressure distribution throughout the bearing (and the bearing load) can be obtained.

To determine the boundary conditions for Equations (2-13) and (2-14), the perturbed mass flows are equated:

$$0(\varepsilon): \qquad m_3^{*} + m_1^{*} = m_2^{*}$$

After substitution of the assumed form of g(x,z,t) given by Equation (2-12) and equating the coefficients of the sine and cosine terms, $g_1(x,z)$ and $g_2(x,z)$ along the inlet boundary are obtained from

$$g_1(x,z) = \frac{2P_oP_s}{\alpha_2(P_o^2-1)F}\left\{\int_o^a \left[\left(\frac{\partial g_1}{\partial z}\right)_{z=b^+} - \left(\frac{\partial g_1}{\partial z}\right)_{z=b^-}\right]dx + \int_o^b \left[\left(\frac{\partial g_1}{\partial x}\right)_{x=a^+} - \left(\frac{\partial g_1}{\partial x}\right)_{x=a^-}\right] dz\right\} + \frac{2P_oP_s}{\alpha_2} \qquad (2\text{-}29)$$

and

$$g_2(x,z) = \frac{2P_oP_s}{\alpha_2(P_o^2-1)F}\left\{\int_o^a \left[\left(\frac{\partial g_2}{\partial z}\right)_{z=b^+} - \left(\frac{\partial g_2}{\partial z}\right)_{z=b^-}\right] dx + \int_o^b \left[\left(\frac{\partial g_2}{\partial x}\right)_{x=a^+} - \left(\frac{\partial g_2}{\partial x}\right)_{x=a^-}\right] dz\right\} \tag{2-30}$$

for $\frac{P_o}{P_s} > \left(\frac{2}{k+1}\right)^{\frac{k}{k-1}}$,

or

$$\int_o^a \left[\left(\frac{\partial g_1}{\partial z}\right)_{z=b^+} - \left(\frac{\partial g_1}{\partial z}\right)_{z=b^-}\right]dx + \int_o^b \left[\left(\frac{\partial g_1}{\partial x}\right)_{x=a^+} - \left(\frac{\partial g_1}{\partial x}\right)_{x=a^-}\right]dz$$

$$= - F(P_o^2-1) \tag{2-31}$$

and

$$\int_o^a \left[\left(\frac{\partial g_2}{\partial z}\right)_{z=b^+} - \left(\frac{\partial g_2}{\partial z}\right)_{z=b^-}\right]dx + \int_o^b \left[\left(\frac{\partial g_2}{\partial x}\right)_{x=a^+} - \left(\frac{\partial g_2}{\partial x}\right)_{x=a^-}\right]dz = 0 \tag{2-32}$$

for $\frac{P_o}{P_s} \leq \left(\frac{2}{k+1}\right)^{\frac{k}{k-1}}$.

2.3 Bearing Load

If the restrictor coefficient is specified, the static pressure distribution can be found from the solution of either Equation (2-27) or Equation (2-28). The static load is then given by

$$W_1 = 4 \int_o^{\lambda/2} \int_o^{1/2} P_1\ (x,z)\ dx\ dz \tag{2-33}$$

where the double integral is taken over the entire quadrant.

Also, given the solutions for $g_1(x,z)$ and $g_2(x,z)$, the dynamic pressure distribution is simply

$$P_2(x,z,t) = \frac{g_1(x,z)}{P_1(x,z)} \sin(t) + \frac{g_2(x,z)}{P_1(x,z)} \cos(t) \quad .$$

The dynamic load is defined by

$$W_2 = 4 \int_0^{\lambda/2} \int_0^{1/2} P_2(x,z,t)\, dx\, dz \tag{2-34}$$

where the double integral is again taken over the quadrant. The dynamic load is then written in the form

$$W_2 = C \sin(t) + B \cos(t) \quad . \tag{2-35}$$

2.4 Stiffness and Damping

If the bearing load executes small harmonic motion, the equation of motion is written

$$W_1^* + \varepsilon W_2^* = W_1^* - K^* Y^* - D^* \frac{dY^*}{dt^*} \tag{2-36}$$

where K^* and D^* are the stiffness and damping constants respectively, and $Y^* = \varepsilon h_o^* \sin(\omega^* t^*)$. Equation (2-36) can be rewritten as

$$W_2 = \frac{W_2^*}{\lambda P_a^* L^{*2}} = - \frac{K^* h_o^*}{\lambda P_a^* L^{*2}} \sin(t) - \frac{D^* h_o^* \omega^*}{\lambda P_a^* L^{*2}} \cos(t) \tag{2-37}$$

By comparison of the above equation with Equation (2-35), dimensionless stiffness and damping can be defined by

$$K_s = -\frac{C}{P_s - 1} = \frac{K^* h_o^*}{\lambda P_a^* L^{*2}(P_s - 1)} \tag{2-38}$$

$$D = -\frac{12B}{\sigma} = \frac{D^*}{\lambda L^* \left(\frac{L^*}{h_o^*} \right)^3 \mu} \tag{2-39}$$

CHAPTER III

IMPLEMENTATION OF THE NUMERICAL METHODS

Due to the boundary conditions and the geometry of the problem, a closed form solution was not found. Several approximate methods were considered without success, and it was necessary to use a finite difference technique to solve the problem. In this chapter, the numerical model which is used to represent the problem is presented.

3.1 The Equations in the Field

The successive-over-relaxation (SOR) method [9] was used to model Equations (2-11), (2-13), and (2-14) in the field. This method was chosen because it offered the advantages of fast convergence and small computer storage. In the SOR method, the most recently computed value at any surrounding node is used when the value at a particular node is computed. A temporary value at a particular node is calculated; then, the weighted average of this value and the old value at the node is taken using an acceleration parameter, and this average is the new value at that node. Central differences are used to represent the partial derivatives. This central difference technique gives a truncation error on the order of the square of the spatial increment, Δx^2 or Δz^2.

Letting $f_{i,j}$ represent $(\overline{P}_1{}^2)_{i,j}$ and the applying the SOR method, Equation (2-11) is modeled as follows:

$$f^*_{i,j} = \frac{1}{2(1+\beta^2)} \left(f^{\alpha}_{i,j+1} + f^{\alpha+1}_{i,j-1} + \beta^2 f^{\alpha}_{i+1,j} + \beta^2 f^{\alpha+1}_{i-1,j}\right) \qquad (3\text{-}1)$$

$$f_{i,j}^{\alpha+1} = \omega_1 f_{i,j}^{*} + (1 - \omega_1) f_{i,j}^{\alpha} \tag{3-2}$$

where $\beta = \Delta x/\Delta y$ and ω_1 is the acceleration parameter.

In order to have the fastest convergence possible, an optimum acceleration parameter, ω_o, must be chosen. Roache [9] gives this parameter for a rectangular field with Dirichlet boundary conditions:

$$\omega_o = 2 \left(\frac{1 - \sqrt{1-\eta}}{\eta} \right) \tag{3-3}$$

where

$$\eta = \left[\frac{\cos\left(\frac{\pi}{I-1}\right) + \beta^2 \cos\left(\frac{\pi}{J-1}\right)}{1 + \beta^2} \right]^2 . \tag{3-4}$$

The acceleration parameter, ω_1, used in Equation (3-2) is the one calculated in Equation (3-3).

Equations (2-13) and (2-14) are modeled as follows:

$$(g_1)_{i,j}^{*} = \frac{1}{2(1+\beta^2)} \Big[(g_1)_{i,j+1}^{\alpha} + (g_1)_{i,j-1}^{\alpha+1} + \beta^2 (g_1)_{i+1,j}^{\alpha} + \beta^2 (g_1)_{i-1,j}^{\alpha+1}$$

$$+ \frac{\Delta x^2 \sigma}{(P_1)_{i,j}} (g_2)_{i,j}^{\alpha} \Big] \tag{3-5}$$

$$(g_1)_{i,j}^{\alpha+1} = \omega_2 (g_1)_{i,j}^{*} + (1-\omega_2)(g_1)_{i,j}^{\alpha} \tag{3-6}$$

$$(g_2)^{*}_{i,j} = \frac{1}{2(1+\beta^2)} [(g_2)^{\alpha}_{i,j+1} + (g_2)^{\alpha+1}_{i,j-1} + \beta^2(g_2)^{\alpha}_{i+1,j} + \beta^2(g_2)^{\alpha+1}_{i-1,j}$$

$$- \Delta x^2\sigma(P_1)_{i,j} - \frac{\Delta x^2\sigma}{(P_1)_{i,j}} (g_1)^{\alpha+1}_{i,j}] \tag{3-7}$$

$$(g_2)^{\alpha+1}_{i,j} = \omega_2(g_2)^{*}_{i,j} + (1 - \omega_2)(g_2)^{\alpha}_{i,j} \tag{3-8}$$

Operations are performed in order from Equation (3-5) through Equation (3-8) for each node (i,j).

Again, an optimum acceleration parameter is needed; however, there is no analytical formula which gives this parameter. Trial and error procedures were used, and the acceleration parameter was found to be sufficiently close to that given by Equation (3-3). Thus, Equation (3-3) was used in all cases to find the needed parameter.

Having modeled the equations in the field, the boundaries must be modeled. In the case of Equations (3-1) and (3-2), the boundaries have constant values, but this is not the case for Equations (3-5) through (3-8). They have Dirichlet boundary conditions at the outer edge, but the conditions along the inlet boundary depend on the mass flow.

3.2 Mass Flow

From mass flow relationships, Equations (2-29) through (2-32) were derived to describe $g_1(x,z)$ and $g_2(x,z)$ at the inlet boundary. The two functions, $g_1(x,z)$ and $g_2(x,z)$, are constant along this boundary, and their values on the boundary can be computed using Simpson's 1/3 Rule and central differences. After rearranging, $g_1(x,z)$ and $g_2(x,z)$ on the boundary are given by

$$(g_1)^{\alpha+1}_{i,j} = C_2 \left\{ \sum_{p}^{N_b} [(g_1)^{\alpha+1}_{p-1,j+1} + (g_1)^{\alpha+1}_{p-1,j+1} + 4[(g_1)^{\alpha+1}_{p,j+1} + (g_1)^{\alpha+1}_{p,j-1}] \right.$$

$$+ (g_1)^{\alpha+1}_{p+1,j+1} + (g_1)^{\alpha+1}_{p+1,j-1}] \frac{\Delta z}{3\Delta x} + \sum_{q}^{N_a} [(g_1)^{\alpha+1}_{i+1,q-1}$$

$$+ (g_1)^{\alpha+1}_{i-1,q-1} + 4[(g_1)^{\alpha+1}_{i+1,q} + (g_1)^{\alpha+1}_{i-1,q}] + (g_1)^{\alpha+1}_{i+1,q+1}$$

$$\left. + (g_1)^{\alpha+1}_{i-1,q+1}] \frac{\Delta x}{3\Delta z} + \frac{2P_oP_s}{\alpha_2} \right\} \tag{3-9}$$

and

$$(g_2)^{\alpha+1}_{i,j} = C_2 \left\{ \sum_{p}^{N_b} [(g_2)^{\alpha+1}_{p-1,j+1} + (g_2)^{\alpha+1}_{p-1,j-1} + 4[(g_2)^{\alpha+1}_{p,j+1} + (g_2)^{\alpha+1}_{p,j-1}] \right.$$

$$+ (g_2)^{\alpha+1}_{p+1,j+1} + (g_2)^{\alpha+1}_{p+1,j-1}] \frac{\Delta z}{3\Delta x} + \sum_{q}^{N_a} [(g_2)^{\alpha+1}_{i+1,q-1}$$

$$+ (g_2)^{\alpha+1}_{i-1,q-1} + 4[(g_2)^{\alpha+1}_{i+1,q} + (g_2)^{\alpha+1}_{i-1,q}] + (g_2)^{\alpha+1}_{i+1,q+1}$$

$$\left. + (g_2)^{\alpha+1}_{i-1,q+1}] \frac{\Delta x}{3\Delta z} \right\} \tag{3-10}$$

for

$$\frac{P_o}{P_s} > \left(\frac{2}{k+1}\right)^{\frac{k}{k-1}}$$

or

$$(g_1)^{\alpha+1}_{i,j} = C_3 \left\{ \sum_{p}^{N_b} [(g_1)^{\alpha+1}_{p-1,j+1} + (g_1)^{\alpha+1}_{p-1,j-1} + 4[(g_1)^{\alpha+1}_{p,j+1} + (g_1)^{\alpha+1}_{p,j-1}] \right.$$

$$+ (g_1)^{\alpha+1}_{p+1,j+1} + (g_1)^{\alpha+1}_{p+1,j-1}] \frac{\Delta z}{3\Delta x} + \sum_{q}^{N_a} [(g_1)^{\alpha+1}_{i+1,q-1}$$

$$+ (g_1)^{\alpha+1}_{i-1,q-1} + 4[(g_1)^{\alpha+1}_{i+1,q} + (g_1)^{\alpha+1}_{i-1,q}] + (g_1)^{\alpha+1}_{i+1,q+1}$$

$$\left. + (g_1)^{\alpha+1}_{i-1,q+1}] \frac{\Delta x}{3\Delta z} + F(P_o^{\,2} - 1) \right\} \tag{3-11}$$

and

$$(g_2)^{\alpha+1}_{i,j} = C_3 \left\{ \sum_{p}^{N_b} [(g_2)^{\alpha+1}_{p-1,j+1} + (g_2)^{\alpha+1}_{p-1,j-1} + 4[(g_2)^{\alpha+1}_{p,j+1} + (g_2)^{\alpha+1}_{p,j-1}] \right.$$

$$+ (g_2)^{\alpha+1}_{p+1,j+1} + (g_2)^{\alpha+1}_{p+1,j-1}] \frac{\Delta z}{3\Delta x} + \sum_{q}^{N_a} [(g_2)^{\alpha+1}_{i+1,q-1}$$

$$+ (g_2)^{\alpha+1}_{i-1,q-1} + 4[(g_2)^{\alpha+1}_{i+1,q} + (g_2)^{\alpha+1}_{i-1,q}] + (g_2)^{\alpha+1}_{i+1,q+1}$$

$$\left. + (g_2)^{\alpha+1}_{i-1,q+1}] \frac{\Delta x}{3\Delta z} \right\} \tag{3-12}$$

for

$$\frac{P_o}{P_s} \le \left(\frac{2}{k+1}\right)^{\frac{k}{k-1}}$$

where $p = 2,4,6,\ldots.N_b$ and $q = 2,4,6,\ldots.N_a$

with

$$C_2 = \frac{2\ P_oP_s}{\alpha_2(P_o^{\ 2} - 1)\ F} \left(\frac{1}{1 + \dfrac{2\ P_oP_s}{\alpha_2(P_o^2 - 1)F} \left(\dfrac{2\Delta zN_b}{\Delta x} + \dfrac{2\Delta xN_a}{\Delta z} \right)} \right)$$

$$C_3 = \frac{1}{\dfrac{2\Delta zN_b}{\Delta x} + \dfrac{2\Delta xN_a}{\Delta z}}$$

Using Simpson's 1/3 Rule and central differences,

$$F = \sum_{p}^{N_b} [f_{p-1,j+1} - f_{p-1,j} + 4(f_{p,j+1} - f_{p,j}) + f_{p+1,j+1} - f_{p+1,j}]$$

$$\frac{\Delta z}{3\Delta x} + \sum_{q}^{N_a} [f_{i+1,q-1} - f_{i,q-1} + 4(f_{i+1,q} - f_{i,q}) + f_{i+1,q+1} - f_{i,q+1}]$$

$$\frac{\Delta x}{3\Delta z}$$

with $p = 2,4,6,\ldots.N_b$ and $q = 2,4,6,\ldots.N_a$.

When solutions for $g_1(x,z)$ and $g_2(x,z)$ through the entire field are found, Simpson's 1/3 Rule is again used to compute C and B for use in Equation (2-35).

CHAPTER IV

ANALYSIS OF THE RESULTS

The design of a thrust bearing is based upon the value of a restrictor coefficient which gives either maximum stiffness or maximum damping. The bearing is analyzed at a small squeeze number for two reasons:

1. Most design work will be done for smaller squeeze numbers ($\sigma < 4$) and the stiffness and damping are insensitive to the small squeeze numbers.
2. For larger squeeze numbers, the stiffness increases and damping decreases [3].

The curves describing the effect of important bearing parameters on load capacity, stiffness, damping, and mass flow are shown for a square bearing ($\lambda = 1$) in Figures 3-14. After an error analysis, these relationships are discussed.

4.1 Error Analysis

In the solution of the problem by finite difference methods, Equations (2-11), (2-13), and (2-14) were modeled using central differences. Due to the truncation of the Taylor series in the development of the finite difference model, there is an error in the numerical model. The error in the model of the equation describing the static pressure distribution is of the order of the product of 10^{-6} and the fourth spatial derivative of the solution. In the case of modeling the coupled equations describing the dynamic pressure distribution, the error is of the order of the product of 10^{-4} and the fourth spatial derivative. These errors are not significant since the fourth spatial derivatives are very small.

Convergence was assumed to have been attained when the absolute value of the maximum change in the field from one iteration to the next was less than some specified change. This change in the solution of the static pressure distribution was on the order of 10^{-3}. In the case of the solution for the dynamic pressure distribution, the maximum change allowable was of the order 10^{-5}.

4.2 Load Capacity

A dimensionless bearing load capacity, W_o, is presented as a function of the restrictor coefficient, Λ, and supply pressure, P_s, in Figures 3-5 for ratios of inlet span to bearing span, r = 0.4, 0.6, 0.8. The dimensionless load capacity is defined by

$$W_o = \frac{W_1^*}{\lambda P_a^* L^{*2}(P_s-1)}$$

where $\lambda = 1$.

At a fixed restrictor coefficient (i.e., a fixed P_o) the load capacity increases with r. The reason is that more of the bearing pad is enclosed by the inlets where the pressure is uniform at P_o (the pressure decays from P_o to 1 across the sill). Little change in load capacity occurs for variations in the restrictor coefficient in the range of very high restrictor coefficients and the range of very low restrictor coefficients for all geometries.

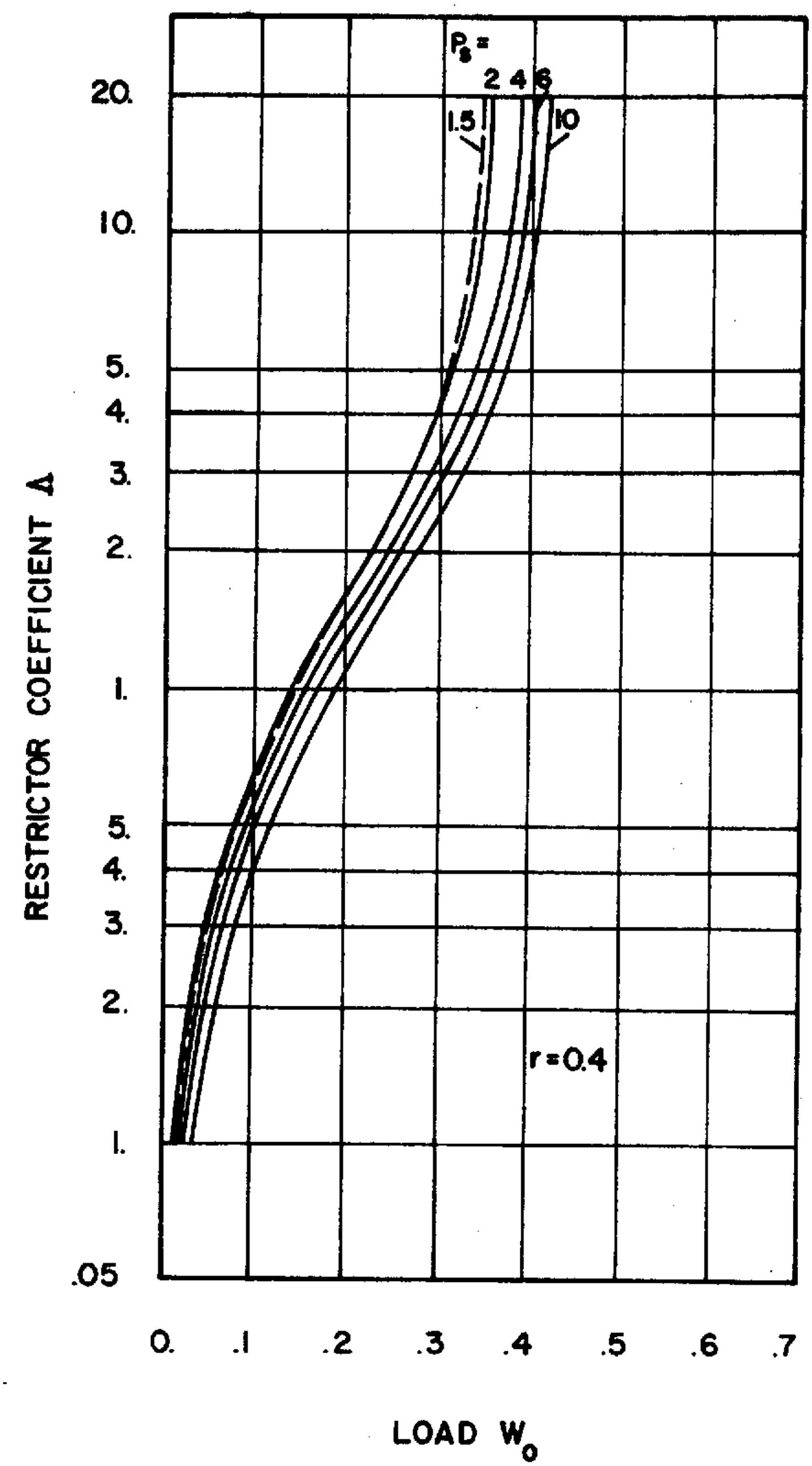

Figure 3. Dimensionless Load Capacity versus Restrictor Coefficient ($r = 0.4$, $\lambda = 1$)

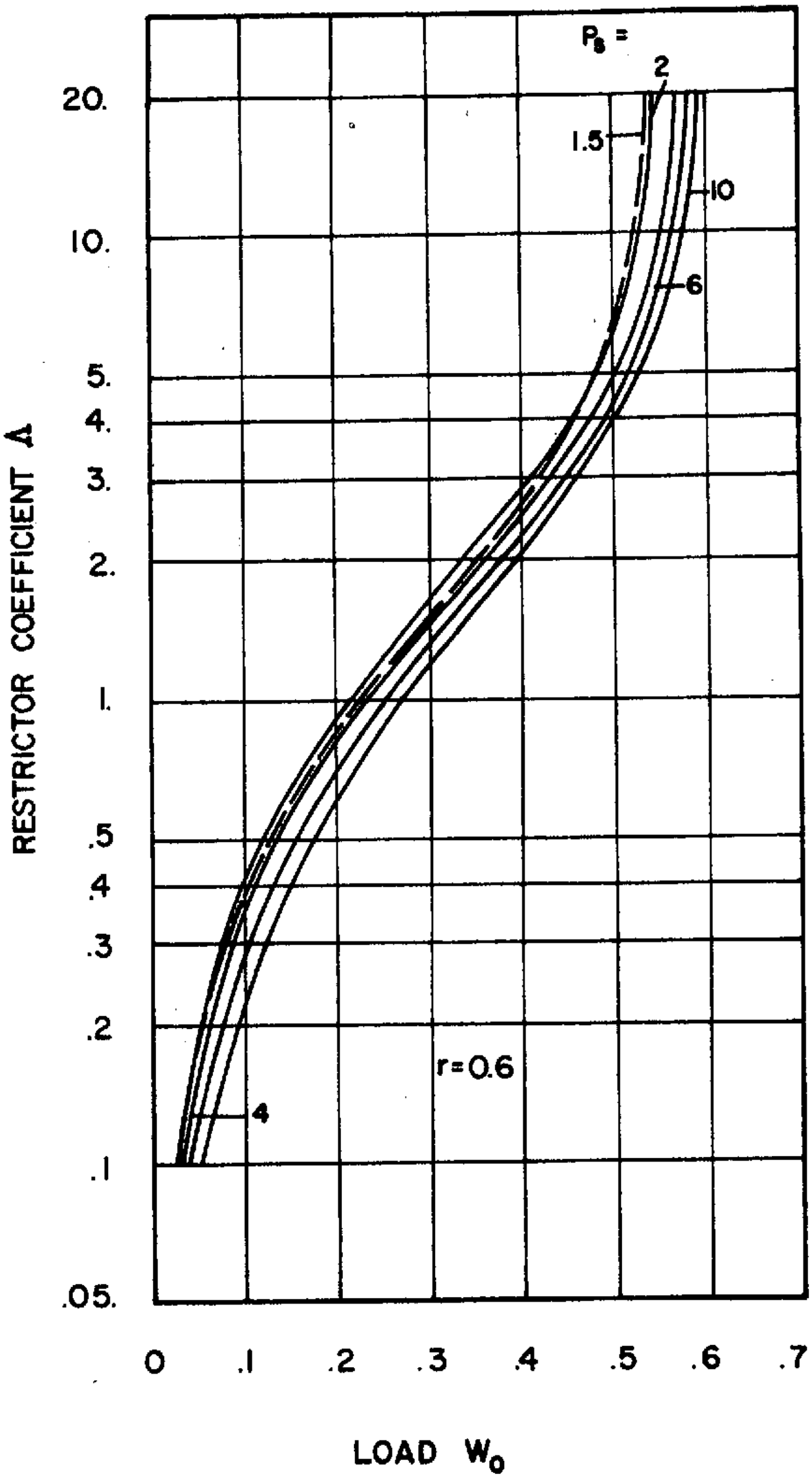

Figure 4. Dimensionless Load Capacity versus Restrictor Coefficient ($r = 0.6$, $\lambda = 1$)

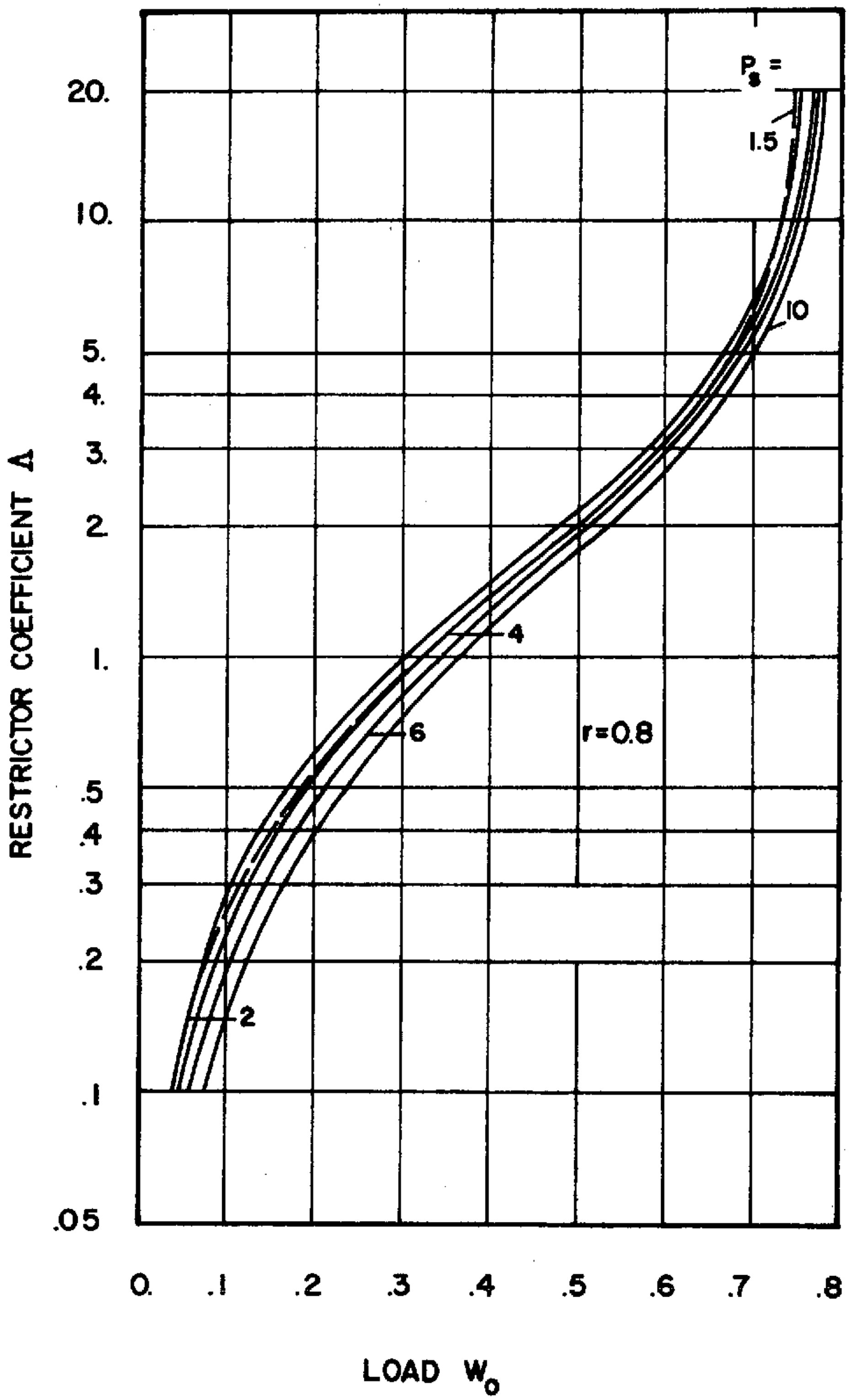

Figure 5. Dimensionless Load Capacity versus Restrictor Coefficient (r = 0.8, λ = 1)

4.3 Damping

The dimensionless damping is very dependent upon the restrictor coefficient for all geometries and supply pressures as can be seen in Figures 6-8. When instability occurs, negative damping is present. The figures show that instability can occur for supply pressures as low as $P_s \simeq 5$, depending upon the inlet location. The range of restrictor coefficient, Λ, for instability varies considerably with geometry. The widest range of instability occurs for the geometry, $r = 0.4$, and the range decreases for increasing r. With high supply pressures, maximum damping occurs in the ranges, $\Lambda \simeq 5$ and $\Lambda < .1$. With low supply pressures, damping approaches a maximum as the restrictor coefficient approaches zero. Within the above ranges, geometry does not have much effect upon the damping. Of course, it is desirable to maintain high stiffness when a design is based upon maximum damping. Thus, the final choice of restrictor coefficient depends upon its relation to the stiffness.

4.4 Stiffness

The relationship between the stiffness, K_s, and the restrictor coefficient, Λ, is shown in Figures 9-11. The stiffness is very sensitive to the restrictor coefficient and is a maximum in the range $1 \leq \Lambda \leq 2$, which is the range where instability occurs for the higher supply pressures. However, at larger values of span ratio, r, instability can be avoided for supply pressures, $P_s < 10$.

Two points should be made:

1. maximum stiffness occurs at values of restrictor coefficients where damping is a minimum; thus, high stiffness and damping are not

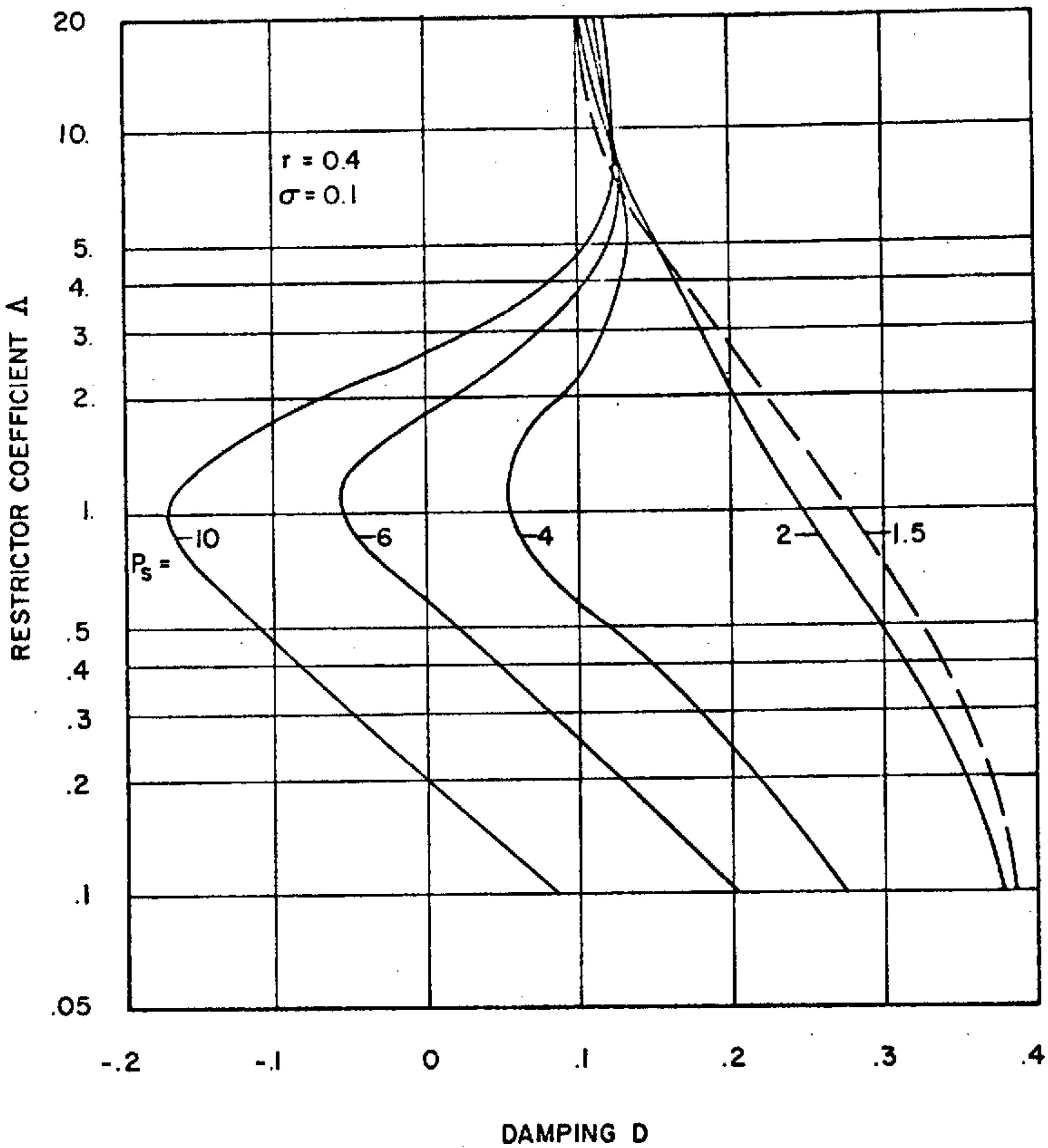

Figure 6. Dimensionless Damping versus Restrictor Coefficient ($r = 0.4$, $\lambda = 1$, $\sigma = 0.1$)

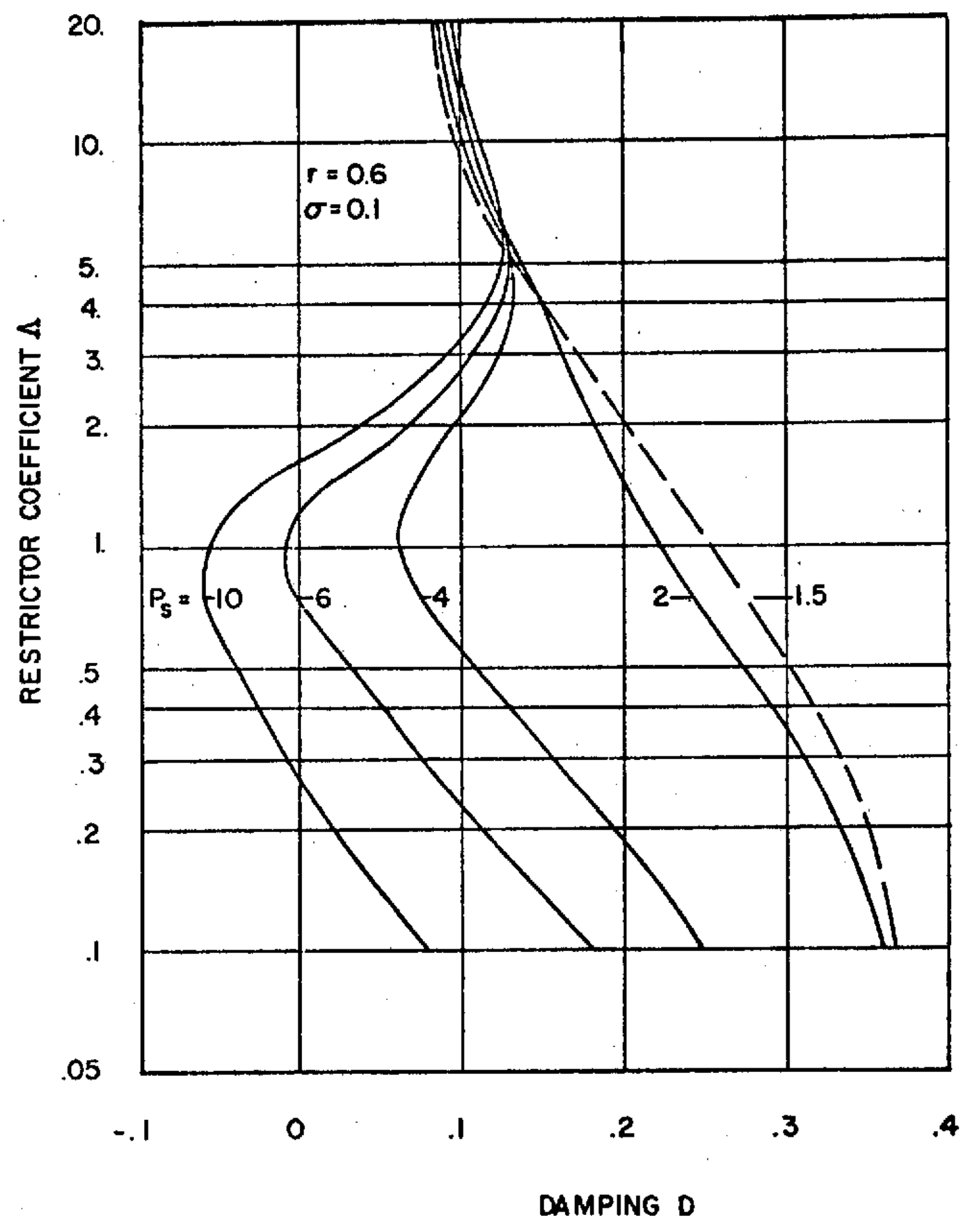

Figure 7. Dimensionless Damping versus Restrictor Coefficient ($r = 0.6, \lambda = 1, \sigma = 0.1$)

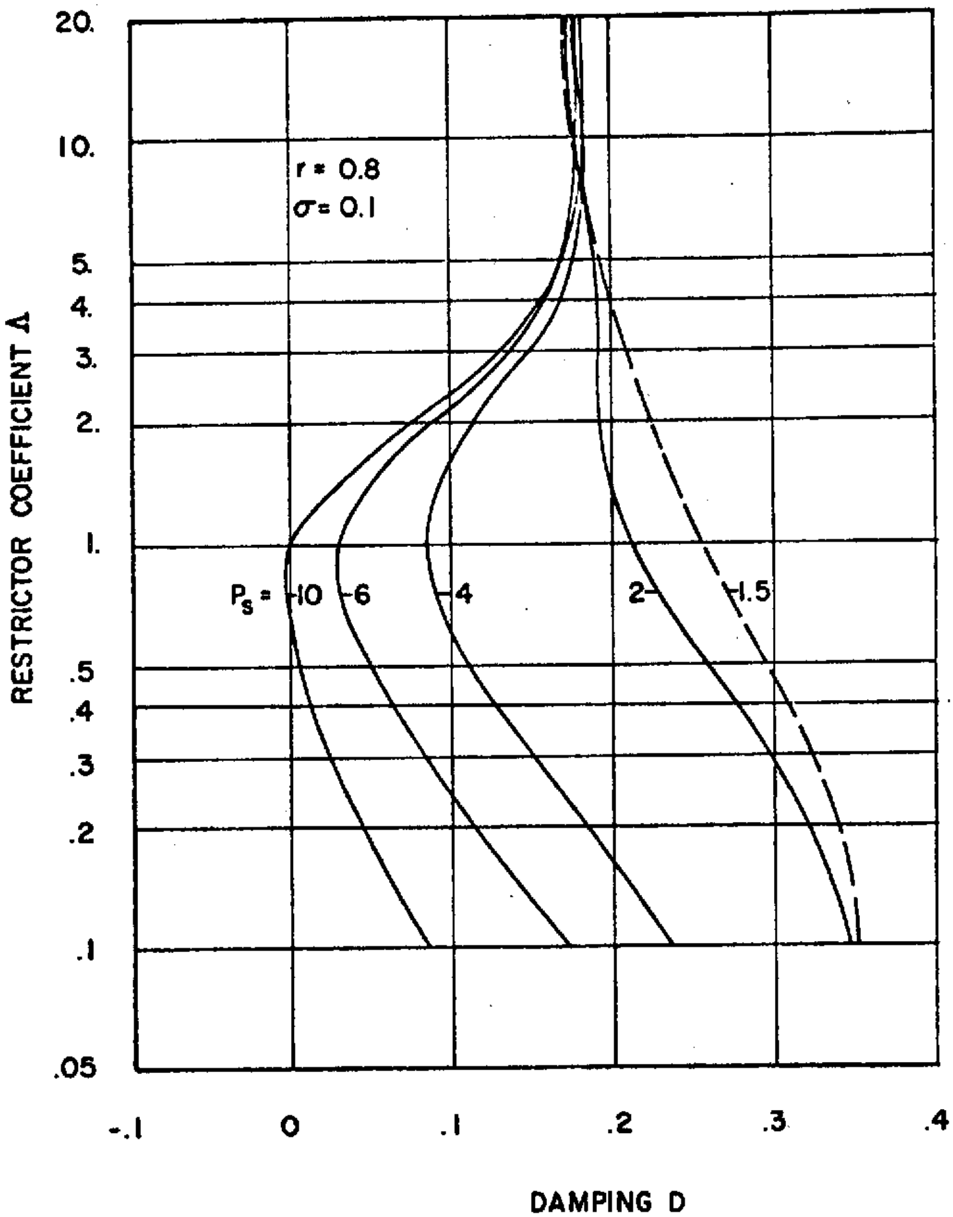

Figure 8. Dimensionless Damping versus Restrictor Coefficient ($r = 0.8$, $\lambda = 1$, $\sigma = 0.1$)

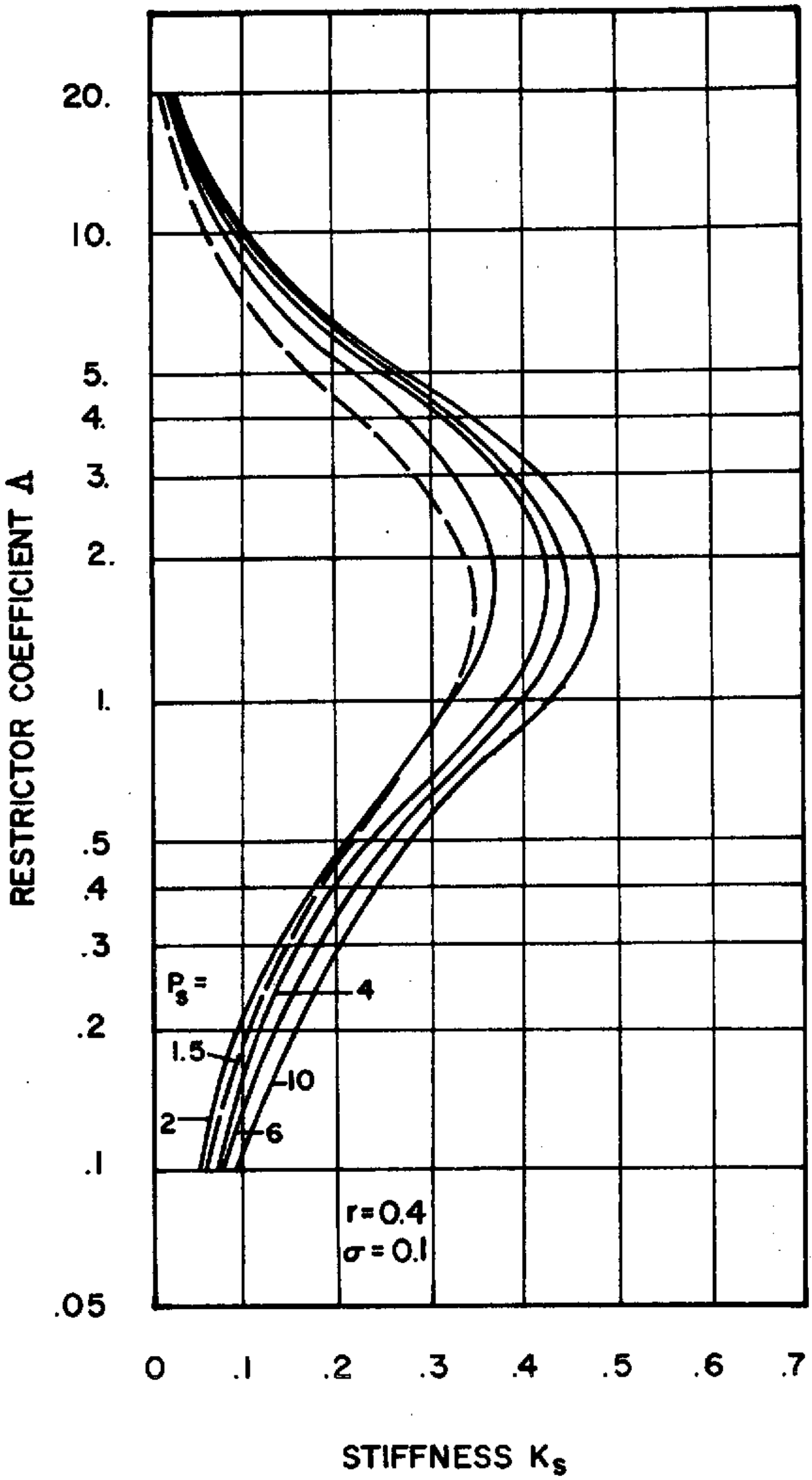

Figure 9. Dimensionless Stiffness versus Restrictor Coefficient ($r = 0.4$, $\lambda = 1$, $\sigma = 0.1$)

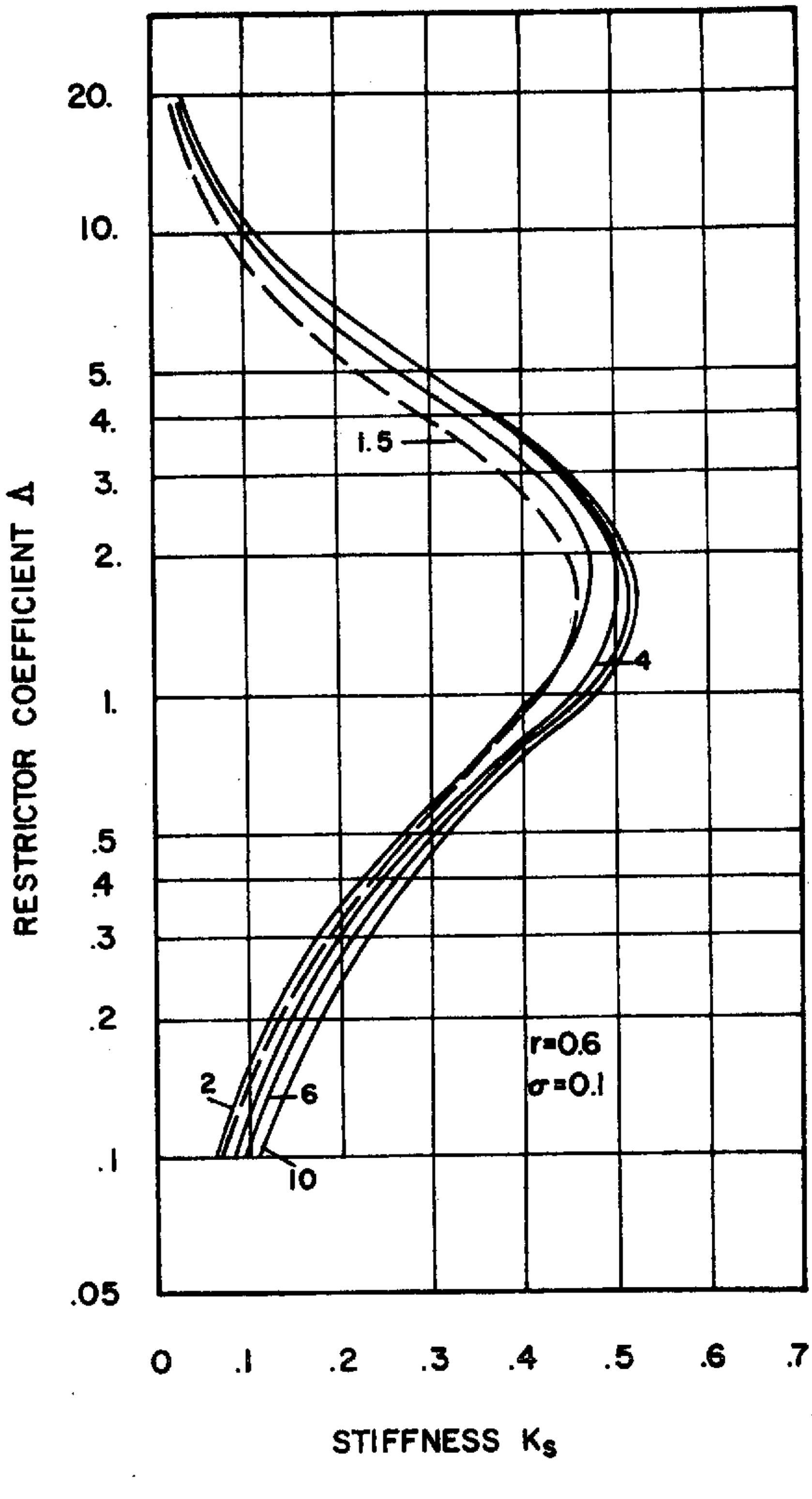

Figure 10. Dimensionless Stiffness versus Restrictor Coefficient ($r = 0.6$, $\lambda = 1$, $\sigma = 0.1$)

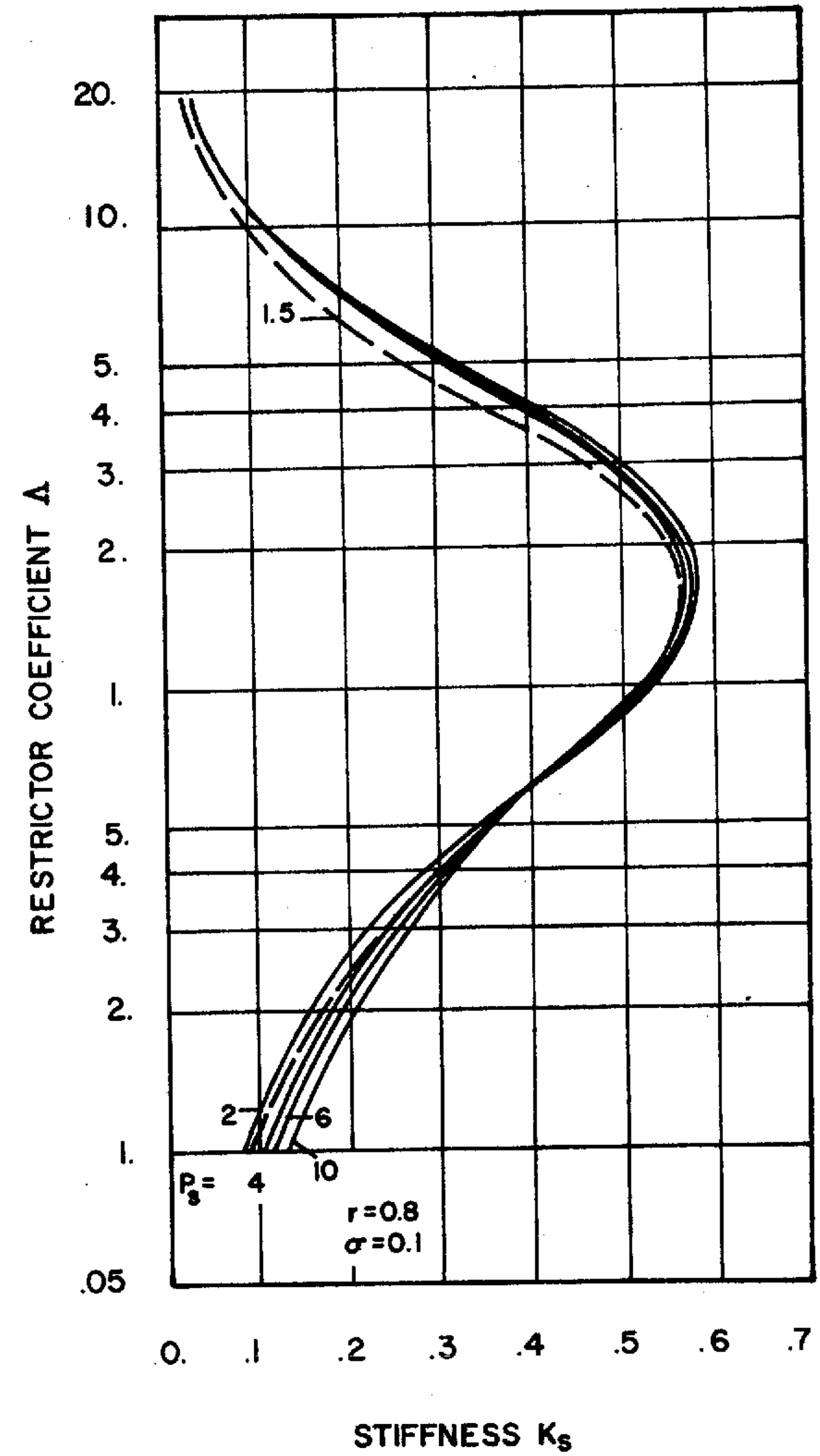

Figure 11. Dimensionless Stiffness versus Restrictor Coefficient ($r = 0.8$, $\lambda = 1$, $\sigma = 0.1$)

compatible;

2. maximum stiffness occurs near the restrictor coefficient value where the flow through the orifice is critical.

As the restrictor coefficient approaches zero, the stiffness also approaches zero although damping is increasing. Thus, when designing for maximum damping, the higher value of $\Lambda = 5$ is generally a better selection.

The stiffness, K_s, also increases as the span ratio, r, increases. Furthermore, K_s is non-dimensionalized by the supply pressure (gage); therefore, the actual stiffness is considerably improved by operating at higher supply pressures.

4.5 Mass Flow

Figures 12-14 contain curves of the mass flow versus restrictor coefficient for the three geometries and various supply pressures. The dimensionless mass flow is defined as

$$m_o = - F(P_o^2 - 1)$$

where F is given for the three different span ratios in the table below:

r	F
0.4	-1.83
0.6	-3.48
0.8	-8.44

The actual mass flow is given by

$$m_o^* = \left(\frac{P_a^{*2} h_o^{*3}}{6\mu RT}\right) m_o$$

Generally speaking, the mass flow does not play a direct part in the

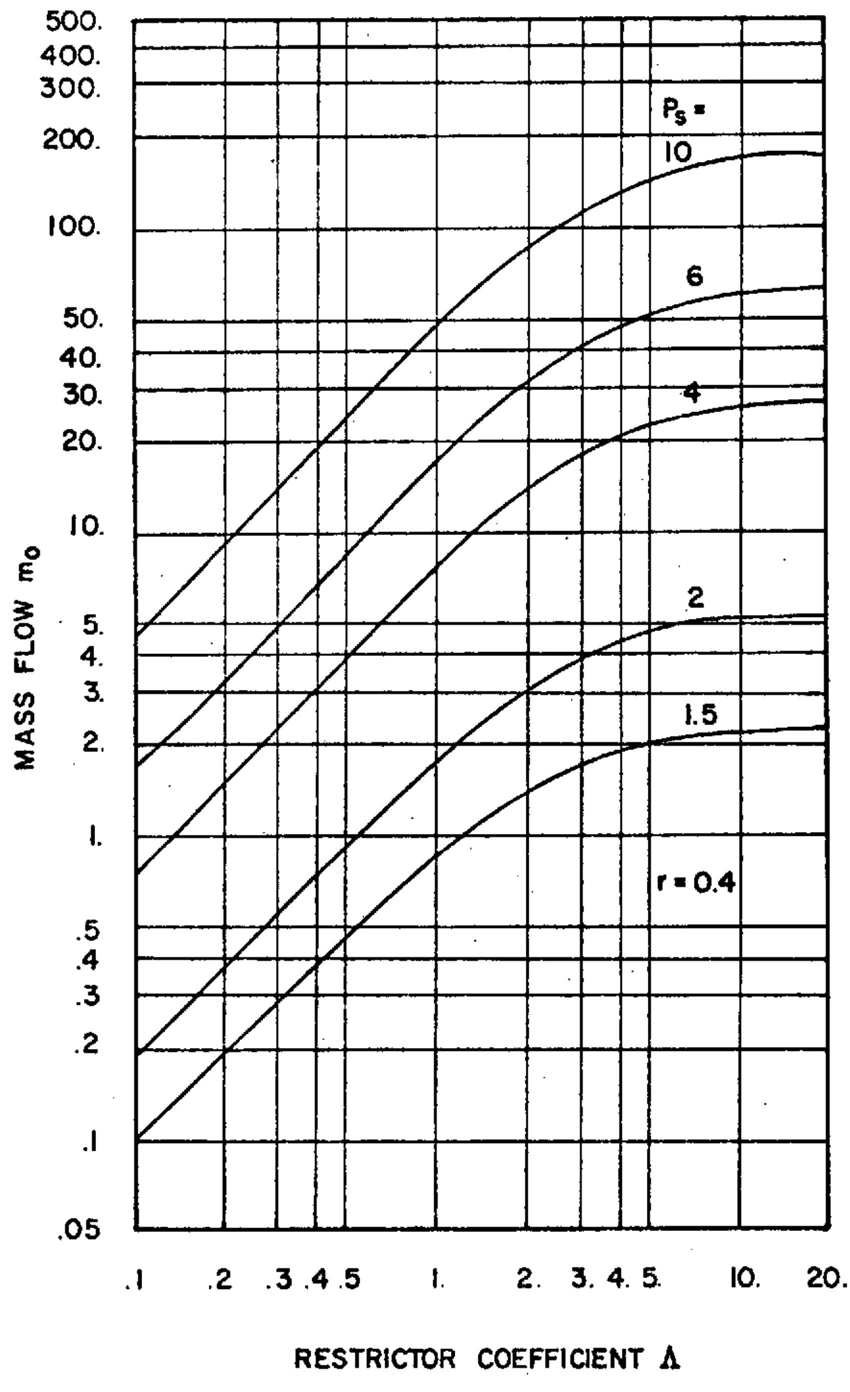

Figure 12. Dimensionless Mass Flow versus Restrictor Coefficient ($r = 0.4$, $\lambda = 1$)

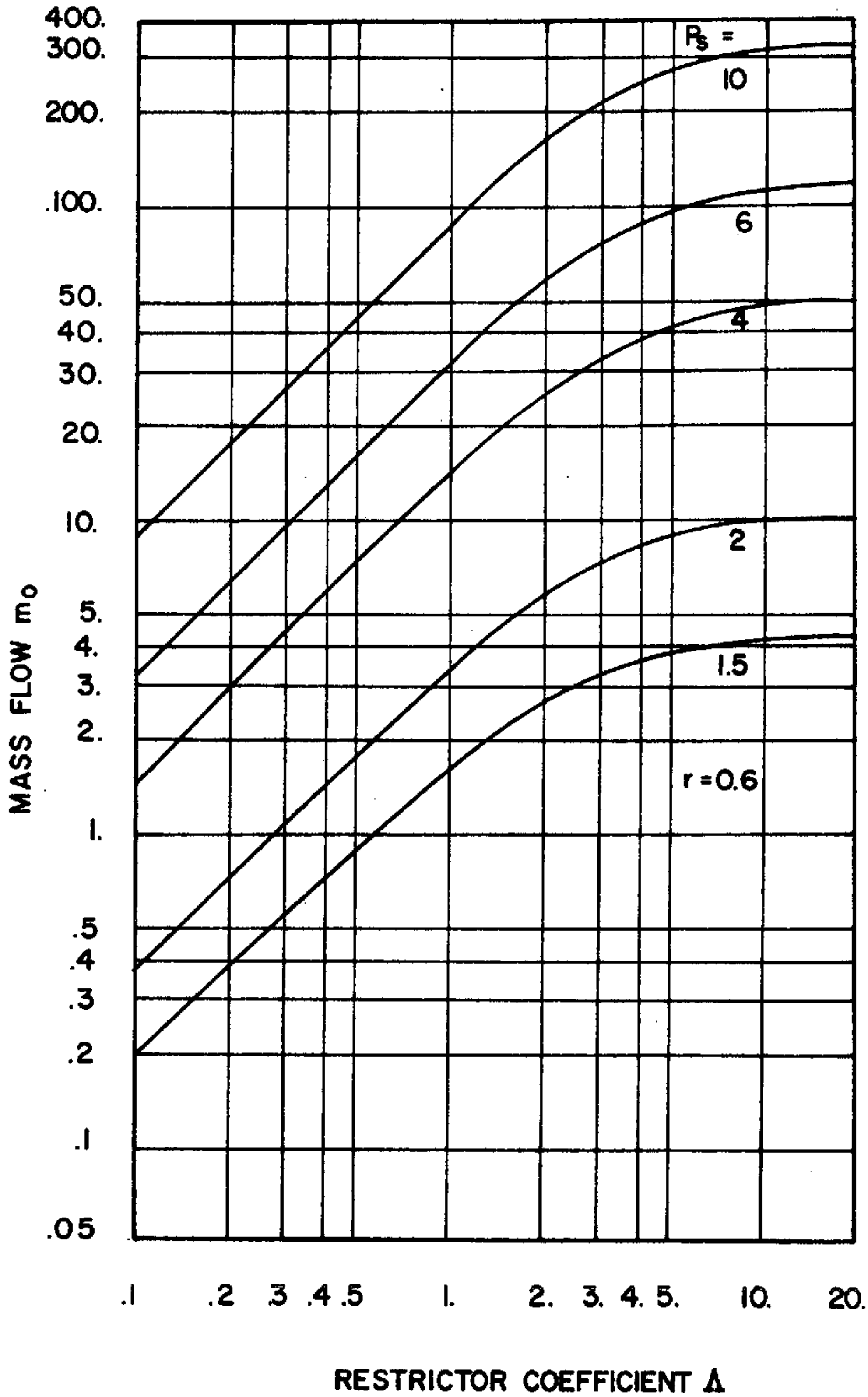

Figure 13. Dimensionless Mass Flow versus Restrictor Coefficient ($r = 0.6$, $\lambda = 1$)

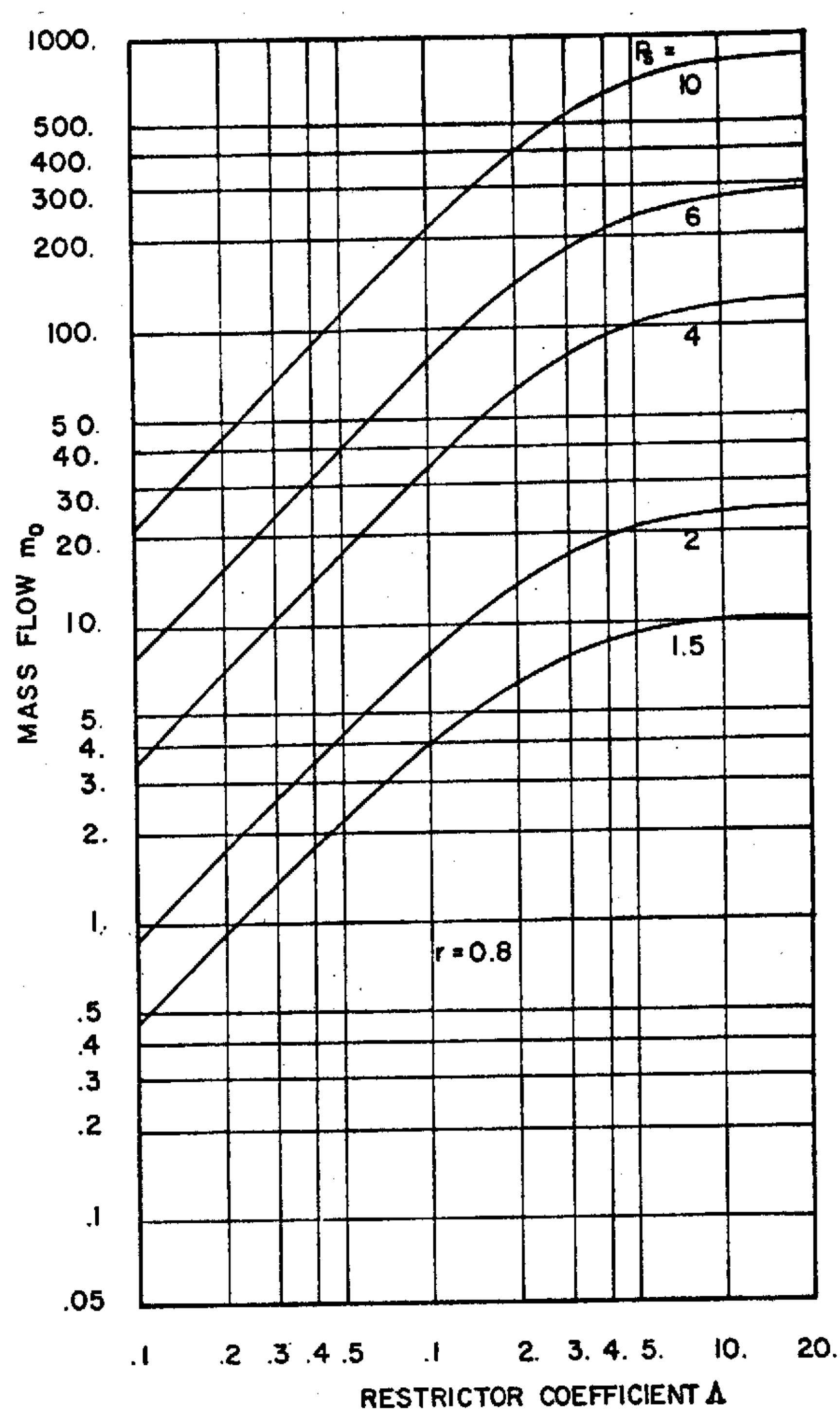

Figure 14. Dimensionless Mass Flow versus Restrictor Coefficient ($r = 0.8$, $\lambda = 1$)

optimum design of the bearing, but this information is necessary for the overall design of the supply system. As a rule, a larger mass flow does increase the frictional losses in the system.

4.6 Squeeze Number

The effect of squeeze number on the stiffness and damping is shown in Figures 14-17. The results include the two restrictor coefficients that most influence the bearing design: $\Lambda = 1.5, 5$. Low squeeze numbers ($\sigma < 10$-20) have little effect on the dynamic characteristics. For large squeeze numbers the damping decreases and the stiffness increases (termination of the curves at high squeeze numbers is due to instability of the numerical solution). As the squeeze number increases, the stiffness reaches a maximum. The reason is that the viscous forces oppose any rapid flow changes through the bearing, and the operation approaches that of a piston inside a closed cylinder. From Equation (1),

$$[ph]_{\sigma \to \infty} = \text{constant}$$

or

$$(p_1 + \varepsilon p_2)(1 + \varepsilon) = \text{constant}$$

Thus, $p_2 = -p_1$. Integrating both sides over the area and using Equations (30), (32), (35), and (36);

$$[K_s]_{\sigma \to \infty} = W_o + 1/(p_s - 1)$$

The above equation is in agreement with the values of stiffness in Figure 15 which reach their maximum.

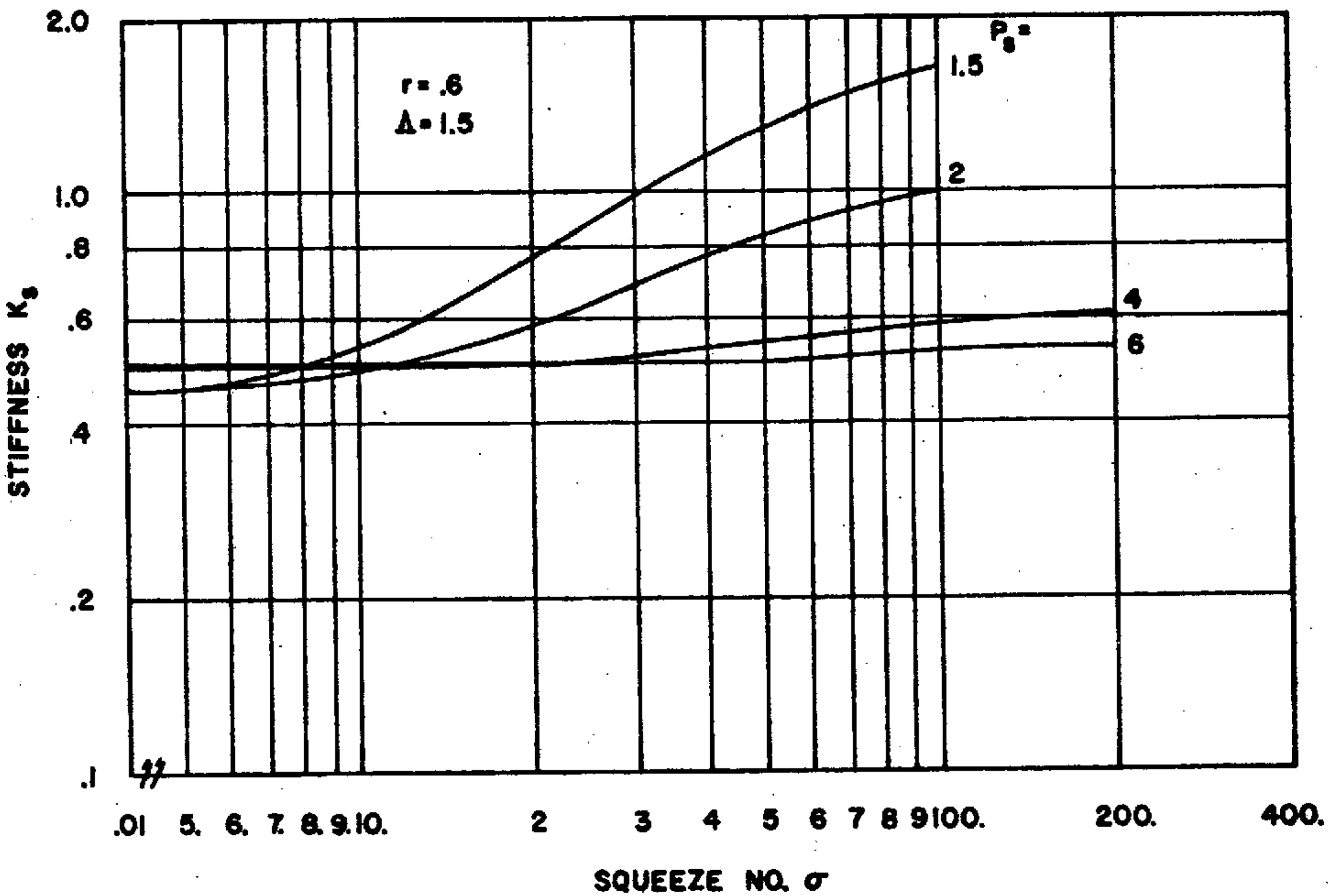

Figure 15. Normalized Stiffness versus Squeeze Number
(Λ = 1.5, r = 0.6, λ = 1)

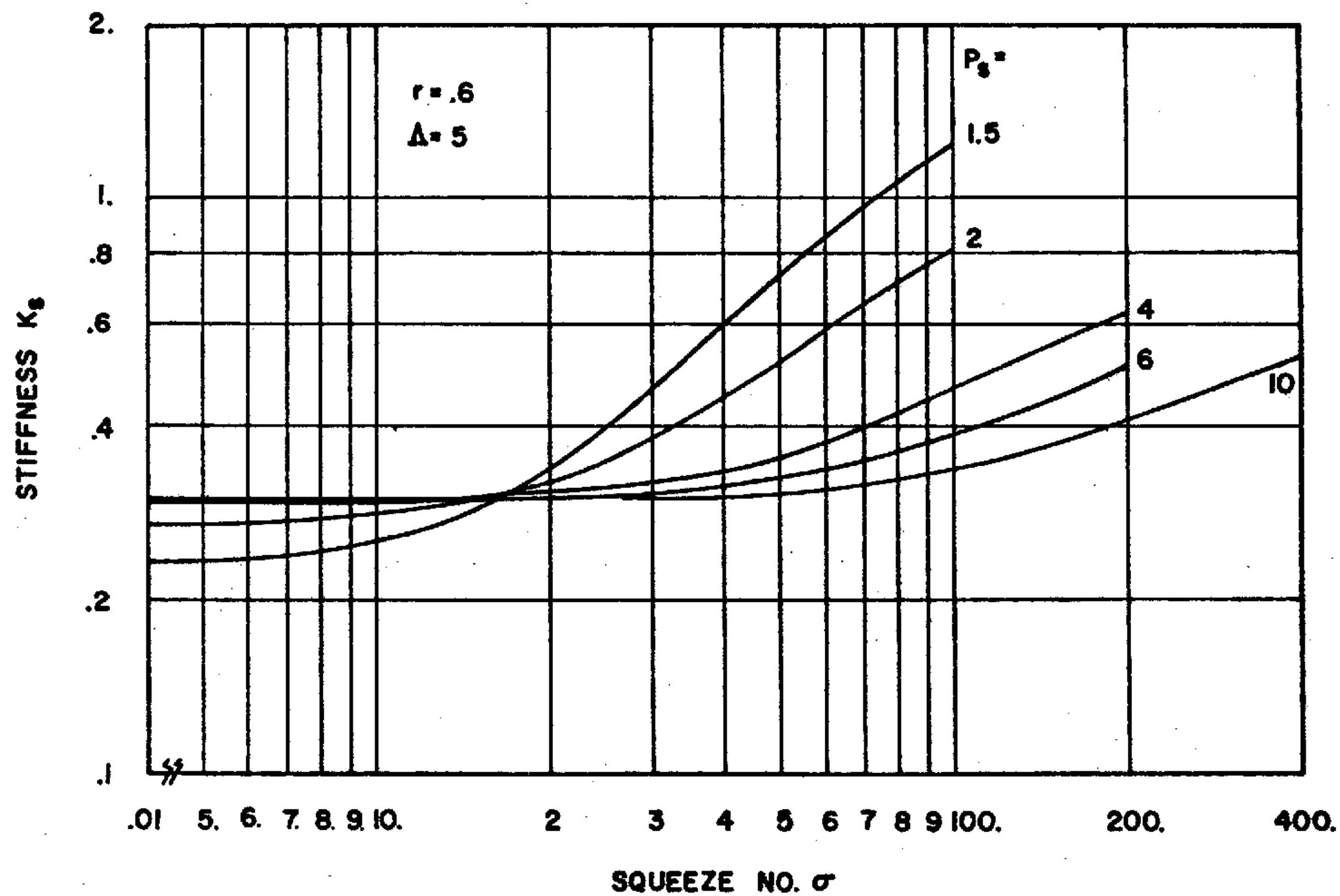

Figure 16. Normalized Stiffness versus Squeeze Number
(Λ = 5, r = 0.6, λ = 1)

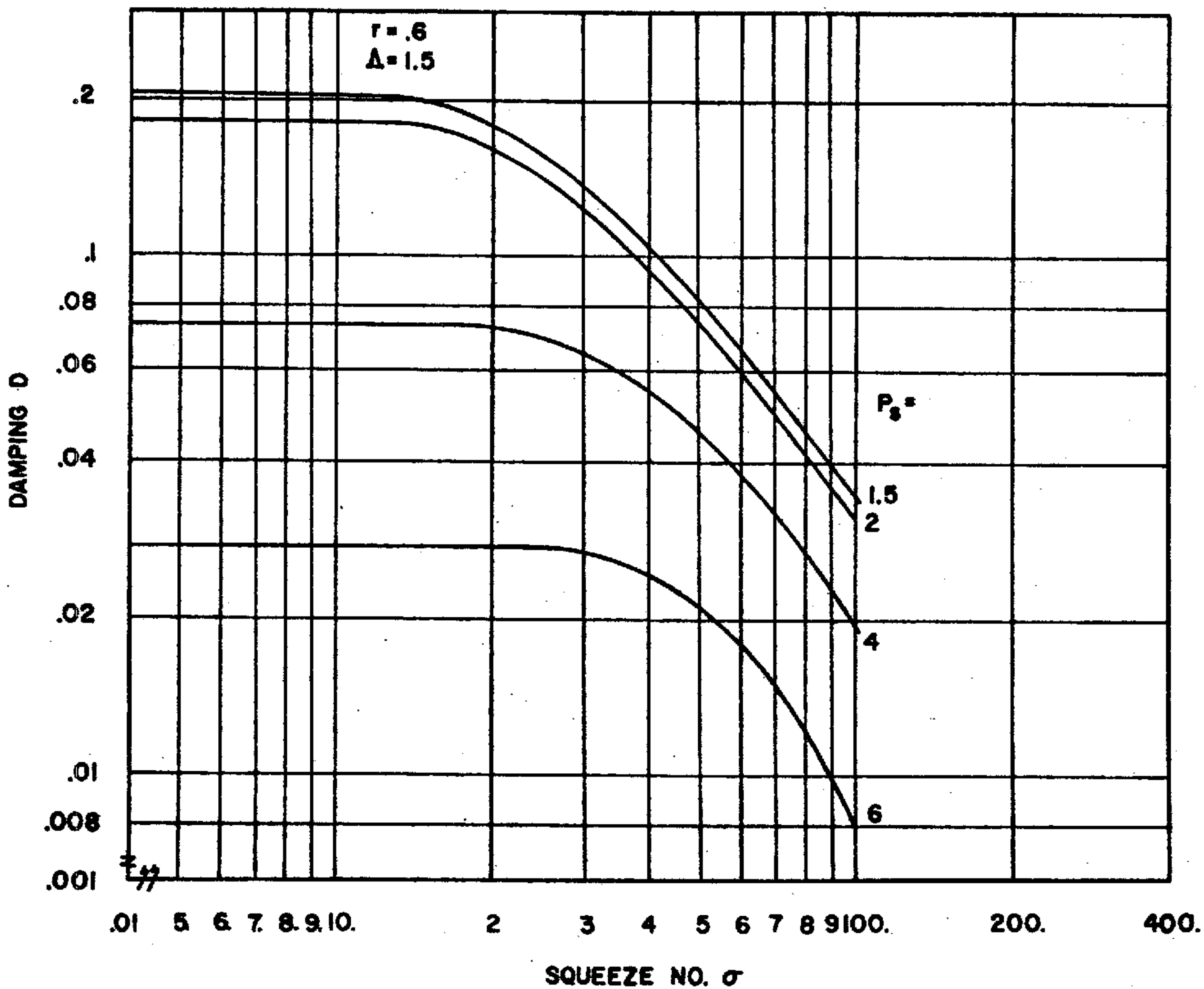

Figure 17. Normalized Damping versus Squeeze Number
(Λ = 1.5, r = 0.6, λ = 1)

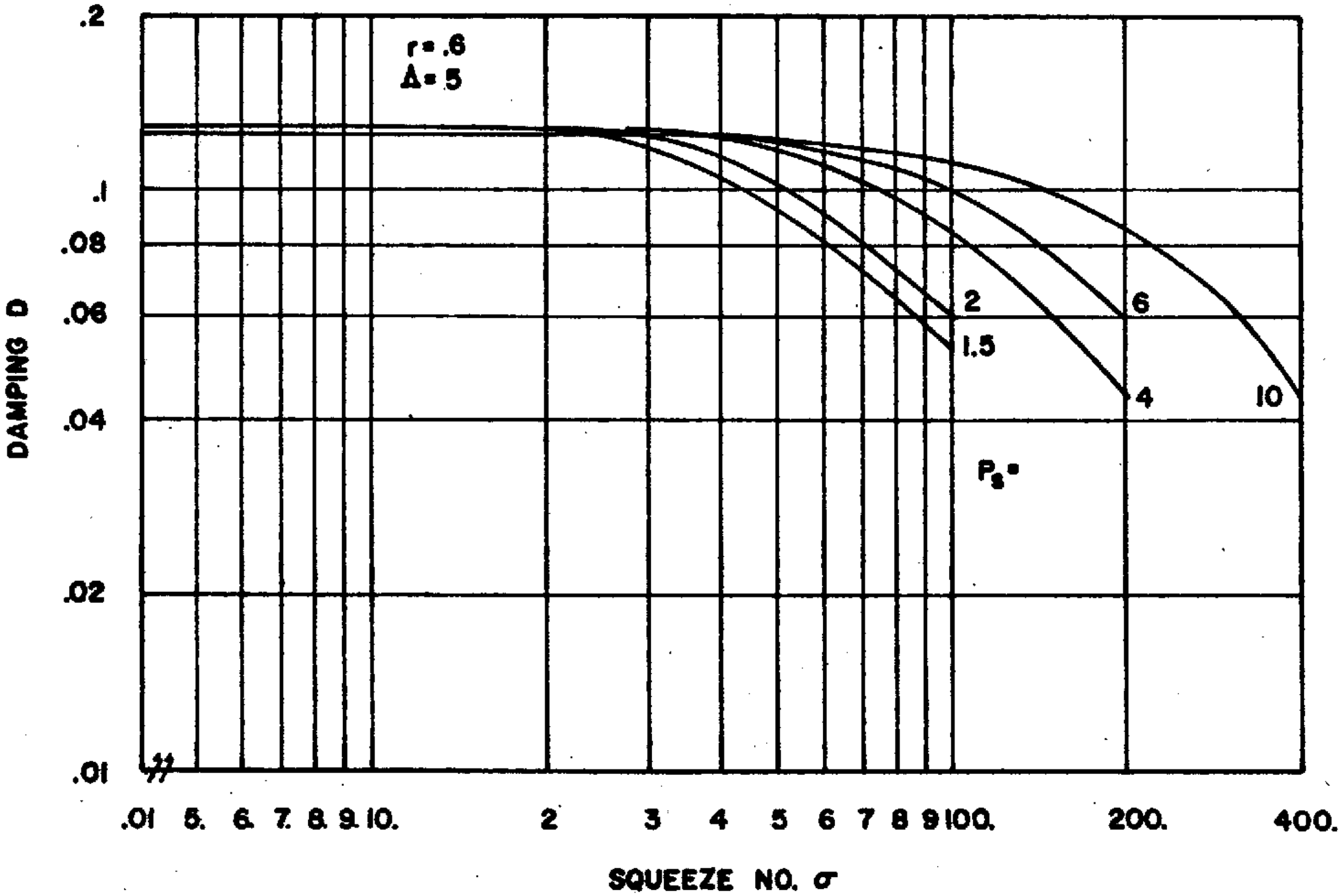

Figure 18. Normalized Damping versus Squeeze Number
($\Lambda = 5$, $r = 0.6$, $\lambda = 1$)

CHAPTER V

CONCLUSIONS AND OPTIMUM DESIGN

The first decision to be made in the design of the bearing is the choice between optimum stiffness and optimum damping. Stiffness is usually the first choice since film thicknesses are on the order of .001 inches and a load disturbance can lead to closure of the bearing if it is too "soft". Furthermore, natural frequencies of the bearing-load system must be avoided. However, damping is necessary when disturbances are present, and many bearings are designed primarily as film dampers. The design procedure is as follows:

1. For maximum stiffness, select a restrictor coefficient, $\Lambda = 1\text{-}2$. Generally, a larger span ratio and a higher supply pressure increase stiffness, but these choices must be weighed against the frictional losses associated with the increased mass flow.
2. The choice of damping is dependent upon the minimum allowable stiffness. Low supply pressures ($P_s = 1.5, 2$) provide high damping for low values of the restrictor coefficient; however, there is a considerable decrease in stiffness. At high supply pressures, damping increases for larger values of the restrictor coefficient. Supply pressure has little effect on damping at higher values of restrictor coefficient, but a higher supply pressure will improve the corresponding stiffness. The damping and stiffness can also be improved by increasing the span ratio. Thus, there are two choices of damping which can be made:
   (a) if low values of stiffness are acceptable, choose a high span ratio with a low supply pressure and a restrictor coefficient

in the range $1 \leq \Lambda \leq 2$;

(b) if higher values of stiffness are needed, choose a high span ratio with a high supply pressure and the restrictor coefficient, $\Lambda = 5$.

3. The choice of restrictor coefficient fixes the dimensionless load capacity. Once the load is specified, the supply pressure determines the bearing dimensions.

It is observed that the dimensionless stiffness and damping are a function of the film thickness. The actual stiffness and damping are improved by the selection of small film thicknesses. Thus, for a fixed restrictor coefficient, the film thickness can be made arbitrarily small by reducing the inlet area of the orifices. In this respect, the designer is limited by the minimum allowable clearance for the bearing.

REFERENCES

1. Richardson, H. H., "Static and Dynamic Characteristics of Compensated Gas Bearings," Trans. ASME, Vol. 80, Oct. 1958, pp. 1503-1509.

2. Licht, L., and Elrod, H., "A Study of the Stability of Externally Pressurized Gas Bearings," Journal of Applied Mechanics, Vol. 27, Trans. ASME, Series E, Vol. 82, 1960, pp. 250-258.

3. Stiffler, A. K., "Analysis of the Stiffness and Damping of an Inherently Compensated, Multiple-Inlet, Circular Thrust Bearing," ASME Paper No. 73-Lub-16.

4. Mullan, P. J., and Richardson, H. H., "Plane Vibration of the Inherently Compensated-Gas Journal Bearing; Analysis and Comparison with Experiment," Journal of Basic Engineering, Trans. ASME, Series D, Vol. 7, 1964, pp. 277-287.

5. Lund, J. W., "A Theoretical Analysis of Whirl Instability and Pneumatic Hammer for a Rigid Rotor in Pressurized Gas Journal Bearings," Journal of Lubrication Technology, Trans. ASME, Series F, Vol. 89, 1967, pp. 154-166.

6. Laub, J. H., "Hydrostatic Gas Bearings," Journal of Basic Engineering, Trans. ASME, Series D, Vol. 82, 1960, pp. 276-286.

7. Constantinescu, V. N. Gas Lubrication. Translated Scripta Technica, Inc. New York: The American Society of Mechanical Engineers, 1969, p. 107.

8. Fleming, D. P., Cunningham, R. E., and Anderson, William J. Stability Analysis for Unloaded Externally Pressurized Gas-Lubricated Bearings with Journal Rotation. NASA TN D-4934, December, 1968.

9. Roache, Patrick J. Computational Fluid Dynamics. 1972; Albuquerque: Hermosa, 1972, pp. 117, 118.

10. Pinkus, Oscar, and Sternlicht, Beno. Theory of Hydrodynamic Lubrication. New York;: McGraw-Hill, 1961, p. 4.

APPENDIX

THE COMPUTER PROGRAM

LUBR*STFFLR.MAIN

```
C       DESCRIBE FIELD AND OBTAIN OMEGA
        DOUBLE PRECISION P0,PS,RST,P1S,X1,ERR1,G1,G2,AL1,AL2
        DIMENSION P1S(52,52),G1(52,52),G2(52,52),
       1P1(51,51)
          REAL LMD,M0
          PI=3.14159
          READ (5,100) G,LMD,M1,M2,N1,N2
          WRITE (6,891)
  891 FORMAT('1',10X,' SIGMA',6X,' P(SUP)',7X,'RST',10X,
     1'P0',10X,'M0',10X,'W0',10X,'F',8X,'STFNESS',6X,'DAMP')
  100     FORMAT(2F10.0,4I3)
          M3=M1+M2
          N3=N1+N2
          FAC=1.0
          DX=0.5/M3
          DY=0.5*LMD/N3
          B=DX/DY
          EPS=((COS(PI/M3)+B**2*COS(PI/N3))/(1.+B**2))**2
          OMG=FAC*2.*((1.-SQRT(1.-EPS))/EPS)
C       DEFINE BOUNDARY CONDITIONS
C       INNER BOUNDARY
        M4=M3+1
        N4=N3+1
        M6=M4+1
        N6=N4+1
        Z4=M4
        X4=N4
        M=M2+1
        N=N2+1
        ML=M+1
        NL=N+1
        DO 1 IA=M,M4
        DO 1 IB=N,N4
      1 P1S(IB,IA)=1.0
        DO 3 IC=1,M4
      3 P1S(1,IC)= 0.0
        DO 4 ID=2,N4
      4 P1S(ID,1)=0.0
        DO 5 IE=2,M2
        DO 5 IF=2,N2
        ZF=IF
        ZE=IE
      5 P1S(IF,IE)=(ZE+ZF)/(M2+N2+1)
        DO 6 IG=2,N2
        DO 6 IH=M,M4
        ZG=IG
      6 P1S(IG,IH)=ZG/(N2+1)
        DO 15 IM=N,N4
        DO 15 IN=2,M2
        ZN=IN
     15 P1S(IM,IN)=ZN/(M2+1)
        DO 820 I9=2,N2
    820 P1S(I9,M4+1)=P1S(I9,M3)
        DO 821 I10=2,M2
    821 P1S(N4+1,I10)=P1S(N3,I10)
```

```
C      ITERATE THRU GAUSS-SEIDEL
         C=0.5/(1.0+B**2)
         C1=B**2
         DO 7 J=1,300
         ERR1=0.0
         Y=0.0
      NN=M4
      DO 10 IK=2,N4
      DO 11 IL=2,NN
         X1=P1S(IK,IL)
      X=C*(P1S(IK,IL+1)+P1S(IK,IL-1)+C1*(P1S(IK+1,IL)
     1+P1S(IK-1,IL)))
         P1S(IK,IL)=OMG*X+(1.0-OMG)*P1S(IK,IL)
      CALL ERROR(P1S,Y,X1,ERR1,M6,N6,IL,IK,IMAX,JMAX)
   11    CONTINUE
      IF (IK.EQ.N2) GO TO 12
         GO TO 10
   12 NN=M2
   10    CONTINUE
      DO 720 I1=2,N2
  720 P1S(I1,M4+1)=P1S(I1,M3)
      DO 721 I11=2,M2
  721 P1S(N4+1,I11)=P1S(N3,I11)
         YF=SQRT(Y)/(M3*N3)
         IF(ERR1-10.**-3) 13,13,7
    7    CONTINUE
   13    CONTINUE
         F=0.0
         C55=DX/(3.0*DY)
         C66=DY/(DX*3.0)
      DO 26 IR=ML,M3,2
   26 F=F+C55*(P1S(N-1,IR-1)+4.*P1S(N-1,IR)+P1S(N-1,IR+1)-
     16.0)
      DO 27 IS=NL,N3,2
   27 F=F+C66*(P1S(IS-1,M-1)+4.*P1S(IS,M-1)+P1S(IS+1,M-1)-
     16.0)
  817 CONTINUE
         READ (5,888) K1,K3,K4,L1,L3,L4
         Q4=K4
         R4=L4
         BY=0.5*LMD/L3
         BX=0.5/K3
  888    FORMAT(6I5)
         DO 31 IA=1,K4
         G2(1,IA)=0.0
   31    G1(1,IA)=0.0
         DO 32 IB=1,L4
         G2(IB,1)= 0.0
   32    G1(IB,1)= 0.0

C   INITIAL GUESSES

         DO 33 IC=2,K4
         DO 33 ID=2,L4
   33    G1(ID,IC)=-(IC+ID)/(Q4+R4)
         MNEW=K4-K1
         NNEW=L4-L1
```

```
      MNEW1=MNEW-1
      NNEW1=NNEW-1
      MNEW2=MNEW+1
      NNEW2=NNEW+1
      MEND=K4-MNEW
      NEND=L4-NNEW
     K6=K4+1
     L6=L4+1
      XNEW=MNEW1
      YNEW=NNEW1
      DO 34 IE=MNEW,K4
      DO 34 IF=NNEW,L4
 34   G2(IF,IE)=0.05-(IF+IE-MNEW-NNEW)*0.1/(Z4+X4)*(-1.)
      DO 35 IG=2,MNEW1
      DO 35 IZ=2,NNEW1
 35   G2(IZ,IG)=(IG+IZ)*0.1/((XNEW+YNEW)*2.)*(-1.)
      DO 36 IJ=2,MNEW
      DO 36 IK=NNEW,L4
 36   G2(IK,IJ)=IJ*0.1/(2.*MNEW)*(-1.)
      DO 37 IL=MNEW,K4
      DO 37 IM=2,NNEW
 37   G2(IM,IL)=IM*0.1/(2.*NNEW)*(-1.)
      C22=BY/(BX*3.0)
      C11=BX/(BY*3.0)
     P0=3.82D0
     DO 81 IJK=1,7
      READ(5,401) PS,SIGM,RST
401   FORMAT(3F10.0)
      IF(RST-30.) 82,83,83
 83   P0=PS-.005D0
 82   CONTINUE
     CALL PLOAD(RST,W0,PS,P0,P1S,P,DX,DY,M,N,M4,N4,N1,M0,F,
    1$25,LMD,N3,M3,P1,M6,N6)
819 CONTINUE
      T=P0/PS
      QT=(2./2.4)**(1.4/0.4)
      IF(T-QT) 94,94,95
 94   AL1=1.
      AL2=F*(P0**2-1.)
      C44=2.*NEND*BY/BX+2.*MEND*BX/BY
      GO TO 96
 95 ALPH=PS/(P0*1.4)-(0.4/2.8)*((PS/P0)**(1./1.4)/
    1(1.-(P0/PS)**(.4/1.4)))
      AL1=2.*PS*P0/(ALPH*(P0**2-1.)*F)
      AL2=2.*PS*P0/ALPH
      C44=1.+AL1*(2.*BY*NEND/BX+2.*BX*MEND/BY)
 96   CONTINUE
      SUM1=0.0
      SUM2=0.0
      DO 41 IR=NNEW2,L3,2
     SUM1=SUM1+C22*(G1(IR-1,MNEW1)+G1(IR-1,MNEW2)+
    14.0*(G1(IR,MNEW1)+G1(IR,MNEW2))+G1(IR+1,MNEW1)+
    1G1(IR+1,MNEW2))
 41 SUM2=SUM2+C22*(G2(IR-1,MNEW1)+G2(IR-1,MNEW2)+
    14.0*(G2(IR,MNEW1)+G2(IR,MNEW2))+G2(IR+1,MNEW1)+
    1G2(IR+1,MNEW2))
      DO 42 IS=MNEW2,K3,2
```

```
      SUM1=SUM1+C11*(G1(NNEW1,IS-1)+G1(NNEW2,IS-1)+
     14.0*(G1(NNEW1,IS)+G1(NNEW2,IS))+G1(NNEW1,IS+1)+
     1G1(NNEW2,IS+1))
   42 SUM2=SUM2+C11*(G2(NNEW1,IS-1)+G2(NNEW2,IS-1)+
     14.0*(G2(NNEW1,IS)+G2(NNEW2,IS))+G2(NNEW1,IS+1)+
     1G2(NNEW2,IS+1))
        IV=K4
        IW=NNEW
   46   DO 47 IT=IW,L4
        DO 47 IU=MNEW,IV
        G1(IT,IU)=(AL1*SUM1+AL2)/C44
        G2(IT,IU)=AL1*SUM2/C44
        IF(IU.EQ.M4) GO TO 45
   47   CONTINUE
        GO TO 48
   45   IV=MNEW
        IW=NNEW2
        GO TO 46
   48   CONTINUE
      DO 815 I1=1,K4
      G1(L4+1,I1)=G1(L4-1,I1)
  815 G2(L4+1,I1)=G2(L4-1,I1)
      DO 816 I2=1,L4
      G1(I2,K4+1)=G1(I2,K4-1)
  816 G2(I2,K4+1)=G2(I2,K4-1)
        B=BX/BY
        C=0.5/(1.0+B**2)
        C1=B**2
      CALL STFDMP(K4,L4,K6,L6,SIGM,C,C1,N4,M4,G1,G2,MNEW,
     1NNEW,MNEW1,MNEW2,NNEW1,NNEW2,ALPH,AL1,AL2,C22,C11,
     1C33,L3,K3,MEND,NEND,P1,PS,BX,BY,P0,F,RST,W0,M0,IMAX,
     1JMAX)
        GO TO 81
   25   WRITE(6,199) PS,SIGM,RST
  199   FORMAT('0','P0.LE.0.OR.GE.PS',3F10.5)
   81   CONTINUE
        STOP
        END
```

LUBR*STFFLR.SUB1

```
      SUBROUTINE  ERROR(P1S,Y,X1,ERR1,M,N,I,J,IMAX,JMAX)
     DOUBLE PRECISION P1S,X1,ERR1,ERR
      DIMENSION P1S(N,M)
      ERR=ABS(P1S(J,I)-X1)
      Y=Y+ERR**2
      IF (ERR-ERR1)1,1,2
    2 ERR1=ERR
      IMAX=I
      JMAX=J
    1 CONTINUE
      RETURN
      END
```

LUBR*STFFLR.SUB2

```
      SUBROUTINE PLOAD(X,W0,PS,X1,P1S,P,DX,DY,M,N,M4,N4,
     1N1,M0,F, $,LMD,N3,M3,P1,M6,N6)
      DOUBLE PRECISION PS,X,X1,Z1,Z2,Z3,FUN,TEST,T1,T2,T3,
     1FP,Y1,P1S
        REAL LMD,M0
      DIMENSION P1S(N6,M6),P1(N4,M4)
        QTESY=(2./2.4)**(1.4/0.4)
        PTEST=PS*QTESY
        IF(X1-PTEST) 4,4,10
   10   CONTINUE
        DO 1 I=1,200
        Z1=X/(X1**2-1.D0)
        Z2=(X1/PS)**(1.D0/1.4D0)
        Z3=DSQRT(1.D0-(X1/PS)**(.4D0/1.4D0))
        FUN=1.D0-Z1*Z2*Z3*PS**2
         TEST=ABS(FUN)
      IF (TEST-0.00001) 2,3,3
    3   T1=2.D0*X1*PS**2/(X1**2-1.D0)
        T2=PS**2*X1**-1/1.4D0
      T3=PS**(2.4D0/1.4D0)*.4D0*X1**(-1.D0/1.4D0)/
     1(2.8D0*Z3**2)
        FP=(T1-T2+T3)*Z1*Z2*Z3
        Y1=X1
        X1=X1-FUN/FP
   98   IF(X1-PS) 11,96,96
   11   IF(X1) 96,96,1
   96   FP=FP*10.D0
        X1=Y1-FUN/FP
        GO TO 98
    1   CONTINUE
    2   CONTINUE
        T=X1/PS
        IF(T-QTESY) 4,4,5
    4   X1=SQRT(1.+X*PS**2*(.4/2.4)**.5*(2./2.4)**2.5)
    5   IF(X1.LE.0.0)  RETURN 16
        DO 6 J=1,M4
        DO 6 K=1,N4
    6   P1(K,J)=SQRT(1.0+(X1**2-1.0)*P1S(K,J)**2)
        W=0.0
        DO 7 L=2,N3,2
        DO 7 IM=2,M3,2
    7 W=W+(DX*DY/9.0)*(P1(L+1,IM+1)+P1(L+1,IM-1)+
     1P1(L-1,IM+1)+P1(L-1,IM-1)+4.*(P1(L,IM+1)+P1(L,IM-1)+
     1P1(L+1,IM)+P1(L-1,IM))+16.*P1(L,IM))
        W0=4.*W
        P=W0/LMD
        M0=-F*(X1**2-1.0)
        W0=(W0-1.)/(PS-1.)
        RETURN
        END
```

```
LUBR*STFFLR.SUB3
      SUBROUTINE STFDMP(M4,N4,M6,N6,SIGM,C,C1,NR,NC,G1,G2,
     1MNEW,NNEW,MNEW1,MNEW2,NNEW1,NNEW2,ALPH,AL1,AL2,C22,
     1C11,C33,N3,M3,MEND,NEND,P1,PS,DX,DY,P0,F,RST,W0,M0,
     1IMAX,JMAX)
      DOUBLE PRECISION P0,PS,RST
     1,G1,G2,SUM1,SUM2,AL1,AL2,XG1,XG2,ERR2,ERR3
      REAL M0
      DIMENSION G1(N6,M6),G2(N6,M6),P1(NR,NC)
      T=P0/PS
      QT=(2./2.4)**(1.4/0.4)
      IF(T-QT)4,4,5
    4 AL1=1.
      AL2=F*(P0**2-1.)
      C44=2.*NEND*DY/DX+2.*MEND*DX/DY
      GO TO 6
    5 ALPH=PS/(P0*1.4)-(0.4/2.8)*((PS/P0)**(1./1.4)/(1.-
     1(P0/PS)**(.4/1.4)))
      AL1=2.*PS*P0/(ALPH*(P0**2-1.)*F)
      AL2=2.*PS*P0/ALPH
      C44=1.+AL1*(2.*DY*NEND/DX+2.*DX*MEND/DY)
    6 CONTINUE
      OM2=1.0
      DO 10 I=1,500
      EG1=0.0
      EG2=0.0
      ERR2=0.0
      ERR3=0.0
      CALL GCMPT(G1,G2,2,M4,2,NNEW1,N4,M4,N6,M6,C,C1,
     1EG1,EG2,ERR2,ERR3,OMG,P1,NR,NC,DX,SIGM,IMAX,JMAX)
      CALL GCMPT(G1,G2,2,MNEW1,NNEW,N4,N4,M4,N6,M6,C,C1,
     1EG1,EG2,ERR2,ERR3,OMG,P1,NR,NC,DX,SIGM,IMAX,JMAX)
      CALL GCMPT(G1,G2,MNEW2,M4,NNEW2,N4,N4,M4,N6,M6,C,C1,
     1EG1,EG2,ERR2,ERR3,OMG,P1,NR,NC,DX,SIGM,IMAX,JMAX)
      SUM1=0.0
      SUM2=0.0
      DO 11 IR=NNEW2,N3,2
      SUM1=SUM1+C22*(G1(IR-1,MNEW1)+G1(IR-1,MNEW2)+
     14.0*(G1(IR,MNEW1)+G1(IR,MNEW2))+G1(IR+1,MNEW1)+
     1G1(IR+1,MNEW2))
   11 SUM2=SUM2+C22*(G2(IR-1,MNEW1)+G2(IR-1,MNEW2)+
     14.0*(G2(IR,MNEW1)+G2(IR,MNEW2))+G2(IR+1,MNEW1)
     1+G2(IR+1,MNEW2))
      DO 12 IS=MNEW2,M3,2
      SUM1=SUM1+C11*(G1(NNEW1,IS-1)+G1(NNEW2,IS-1)+
     14.0*(G1(NNEW1,IS)+G1(NNEW2,IS))+G1(NNEW1,IS+1)
     1+G1(NNEW2,IS+1))
   12 SUM2=SUM2+C11*(G2(NNEW1,IS-1)+G2(NNEW2,IS-1)+
     14.0*(G2(NNEW1,IS)+G2(NNEW2,IS))+G2(NNEW1,IS+1)+
     1G2(NNEW2,IS+1))
      IV=M4
      IW=NNEW
   16 DO 17 IT=IW,N4
      DO 17 IU=MNEW,IV
      XG1=G1(IT,IU)
      XG2=G2(IT,IU)
      G1(IT,IU)=(AL1*SUM1+AL2)/C44
```

```
           G2(IT,IU)=AL1*SUM2/C44
           G1(IT,IU)=OM2*G1(IT,IU)+(1.-OM2)*XG1
           G2(IT,IU)=OM2*G2(IT,IU)+(1.-OM2)*XG2
           CALL ERROR(G1,EG1,XG1,ERR2,M6,N6,IU,IT,IMAX,JMAX)
           CALL ERROR(G2,EG2,XG2,ERR3,M6,N6,IU,IT,IMAX,JMAX)
           IF(IU.EQ.M4) GO TO 15
   17      CONTINUE
           GO TO 18
   15      IV=MNEW
           IW=NNEW2
           GO TO 16
   18      CONTINUE
        DO 815 I1=1,M4
        G1(N4+1,I1)=G1(N4-1,I1)
  815   G2(N4+1,I1)=G2(N4-1,I1)
        DO 816 I2=1,N4
        G1(I2,M4+1)=G1(I2,M4-1)
  816   G2(I2,M4+1)=G2(I2,M4-1)
          EG1=SQRT(EG1)/(M3*N3)
          EG2=SQRT(EG2)/(M3*N3)
        IF (ERR2-.5*10.**-3) 19,10,10
   19   IF (ERR3-.5*10.**-3) 20,10,10
   10   CONTINUE
   20     CONTINUE
          W21=0.0
          W22=0.0
          CONST=DX*DY/9.0
          DO 1 J=2,M3,2
          DO 1 K=2,N3,2
        W21=W21+CONST*(G1(K+1,J+1)/P1(K+1,J+1)+G1(K+1,J-1)
      1/P1(K+1,J-1)+G1(K-1,J+1)/P1(K-1,J+1)+G1(K-1,J-1)
      1/P1(K-1,J-1)+4.*(G1(K,J+1)/P1(K,J+1)+G1(K,J-1)
      1/P1(K,J-1)+G1(K+1,J)/P1(K+1,J)+G1(K-1,J)/P1(K-1,J))+
      116.*G1(K,J)/P1(K,J))
    1 W22=W22+CONST*(G2(K+1,J+1)/P1(K+1,J+1)+G2(K+1,J-1)
      1/P1(K+1,J-1)+G2(K-1,J+1)/P1(K-1,J+1)+G2(K-1,J-1)
      1/P1(K-1,J-1)+4.*(G2(K,J+1)/P1(K,J+1)+G2(K,J-1)
      1/P1(K,J-1)+G2(K+1,J)/P1(K+1,J)+G2(K-1,J)/P1(K-1,J))+
      116.*G2(K,J)/P1(K,J))
          W21=4.*W21
          W22=4.*W22
          STIFF=-W21/(PS-1.)
          DAMP=-12.*W22/SIGM
          WRITE (6,889) SIGM,PS,RST,P0,M0,W0,F,STIFF,DAMP
  889     FORMAT('0',5X,9E12.3)
          RETURN
          END
```

```
LUBR*STFFLR.SUB4
             SUBROUTINE GCMPT(G1,G2,J,K,M,N,N4,M4,N6,M6,C,C1,EG1,
            1EG2,ERR2,ERR3,OMG,P1,NR,NC,DX,SIGM,IMAX,JMAX)
             DOUBLE PRECISION G1,G2,XG1,XG2,XG,YG,ERR2,ERR3
               DIMENSION G1(N6,M6),G2(N6,M6),P1(NR,NC)
             PI=3.14159
               DO 1 I=J,K
               DO 1 L=M,N
             C2=SIGM*DX**2/P1(L,I)
             C3=SIGM*P1(L,I)*DX**2
             XMU=2.*(COS(PI/(2.*M4-1.))+COS(PI/(2.*N4-1.)))
             RHO=((C2*DX**2+SQRT(C2**2*DX**4+16.*XMU))**2)/64.
             OMG=2./(1.+SQRT(1.-RHO**2))
             XG1=G1(L,I)
               XG2=G2(L,I)
             XG=C*(G1(L,I+1)+G1(L,I-1)+C1*(G1(L+1,I)+G1(L-1,I))+
            1C2*G2(L,I))
               G1(L,I)=OMG*XG+(1.-OMG)*G1(L,I)
             YG=C*(G2(L,I+1)+G2(L,I-1)+C1*(G2(L+1,I)+G2(L-1,I))-
            1C3-C2*XG1)
               G2(L,I)=YG*OMG+(1.-OMG)*G2(L,I)
               CALL ERROR(G1,EG1,XG1,ERR2,M6,N6,I,L,IMAX,JMAX)
               CALL ERROR(G2,EG2,XG2,ERR3,M6,N6,I,L,IMAX,JMAX)
         1     CONTINUE
               RETURN
               END

@PCH,S  STFFLR.MAIN

@PCH,S  STFFLR.SUB1

@PCH,S  STFFLR.SUB2

@PCH,S  STFFLR.SUB3

@PCH,S  STFFLR.SUB4

@FIN
```